Lifetime and Growing Process of Localized Turbulence in Plane Channel Flow

Takahiro KANAZAWA

MARCH 2018

Lifetime and Growing Process of Localized Turbulence in Plane Channel Flow

A dissertation submitted to
THE GRADUATE SCHOOL OF ENGINEERING SCIENCE
OSAKA UNIVERSITY
in partial fulfillment of the requirements for the degree of
DOCTOR OF PHILOSOPHY IN ENGINEERING

By

Takahiro KANAZAWA

MARCH 2018

Abstract

In wall-bounded shear flows, the subcritical transition to turbulence is widely observed, and it is triggered by finite-amplitude disturbances beyond certain critical amplitude. Although subcritical turbulence transition has long been investigated, because of fully nonlinear dynamics its details have not been theoretically clarified yet. In our study, we consider the direct numerical simulation (DNS) of plane channel flow with a large numerical domain. Our goal is to describe the growing process to turbulence from a localized perturbation.

First, we carry out the DNS in narrow spanwise numerical domain and measure mean lifetimes of streamwise localized turbulence to discuss the relationship to the number of coherent structure. Increasing the Reynolds number and the spanwise length of the domain, the lifetime becomes longer. Consequently, the mean lifetime at a certain Reynolds number increases exponentially as a function of the number of coherent structures. This indicates that each coherent structure contributes to the lifetime independently.

Secondly, in phase space, there might exist an invariant solution, such as a fixed point and a periodic orbit, to a subcritical Navier-Stokes system. We investigate an invariant solution called an edge state which has only one unstable direction, representing a critical amplitude in subcritical transition. By using edge tracking algorithm and Newton-Krylov hookstep iteration, we have found a spatially localized edge state in the streamwise and spanwise directions. The unstable eigenfunction of the solution shows the appearance of the new low-speed streak, so that turbulence spreads in the spanwise direction. This observation suggests that the instability of the edge state represents the growing process of a turbulent spot.

Thirdly, a two-dimensionally localized turbulent band has been investigated in plane channel flow with a very large numerical domain. The downstream edge region of the band is expected to be responsible for its sustaining mechanism. We extract this region by imposing spatially localized damping force on the Navier-Stokes equations. For a certain value of the damping parameter, a pair of periodic solutions arise from a saddle-node bifurcation at a finite value of the Reynolds number. The solutions could reproduce typical flow structures, i.e. a high-velocity patch and an array of counter-rotating vortex tubes, of a turbulent band in its downstream edge. Reducing the damping force, the stable periodic solution becomes unstable and subsequently, a chaotic solution appears to exhibit a longer array of complex vortices representing the full turbulent band.

Contents

Chapter 1

Introduction

1.1 Transition to turbulence

The flow of fluid is largely divided into laminar flow which has no eddies or unstable structures and turbulence which is observed as spatiotemporal complex dynamics. In wall-bounded shear flow, characteristics of turbulence include strong frictional drag and high heat transport efficiency. If we understand turbulence phenomena, we can realize laminar flow and turbulent state according to circumstances, for example, the drag reduction or heat transfer enhancement, and apply to engineering applications.

As one of many unresolved problems about turbulence, there is the transition from laminar to turbulence. Reynolds (1883)[1] has reported that in pipe flow, the state of the flow depends on one parameter which is now called Reynolds number and turbulence appears when it goes beyond some critical value. There have been two types of such drastic changes of state depending on systems. One of them is a supercritical transition, for example in Taylor-Couette flow or Rayleigh-Bénard convection, which corresponds to a gradual change by increase of Reynolds number. This is known as a simple transition process in which the final state is determined without depending on initial conditions. On the other hand, in many other wall-bounded shear flows like pipe flow or plane channel flow, turbulence can be observed even at low Reynolds number where a laminar state is stable. That is called a subcritical transition caused by a finite amplitude disturbance and its details have not been clarified because of fully nonlinear dynamics.

1.2 Turbulence in the transitional regime

If the Reynolds number is in the transitional regime between laminar flow and turbulent state, the state of flow can have different properties from high Reynolds number turbulence, that is, spatially localized turbulence is observed. In pipe flow or square duct flow, streamwise localized turbulence has been called a turbulent

puff (Wygnansky and Champagne 1973[2]) and growing mechanisms like a splitting (Avila *et al.* 2011[3]; Shimizu *et al.* 2014[4]) or a slugging (Duguet *et al.* 2010[5]) and self-sustaining mechanisms (Shimizu and Kida 2009[6]) have been investigated. In plane channel flow or plane Couette flow, more complex turbulence can be formed because of high freedom degrees. Caused by a local disturbance, a turbulent spot localized in two spatial direction has been observed (Carlson *et al.* 1982[7]). Further growing of a disturbance, a turbulent band inclined in the streamwise direction can be observed (Tsukahara *et al* 2005[8]; Tuckerman and Barkley 2011[9]; Manneville 2011[10]). These patterns depend on the Reynolds number. The higher the Reynolds number, the more the spatial intermittency is lost and finally fully developed turbulence is observed. The critical value where the behavior of turbulence changes has not been specified and it is one of the transition problems mentioned in the previous section 1.1.

Then, localized turbulence has another property. It can indicate a sudden decay to laminar state in a finite time, that is, it has a lifetime. The Reynolds number dependence of lifetimes of transient turbulence has been investigated in pipe flow (Hof *et al.* 2008[11]; Avila *et al.* 2010[12]). In addition, identifying the origin of the transient turbulence is a very important subject of study in the subcritical problem since it will specify the origin of the turbulence (see also next section 1.3).

1.3 Dynamical approaches

As an approach to subcritical transition to turbulence, searching an invariant solution numerically can be conceivable. It is considered that a cloud of periodic orbits is embedded inside the chaotic dynamics like turbulent motions. In previous study, freedom degrees have been reduced by considering a small numerical domain and it is devised that periodic orbits embedded in complex motions can be identified easily. Therefore, an attempt to understand turbulence phenomena by identified dynamics has begun. Then, various invariant solutions have been reported including in plane channel flow (Toh and Itano 2003[13]; Waleffe 2003[14]) or plane Couette flow (Nagata 1990[15]; Kawahara & Kida 2001[16]).

In recent years, development of numerical computational science enables high speed and large scale simulation. More precise discussion in smaller systems (Kreilos and Eckhardt 2012[17]; Shimizu *et al.* 2012[18]; Zammert and Eckhardt 2017[19]) and identification of spatial localized solution in large domain (Avila *et al.* 2013[20]; Brand and Gibson 2015[21]; Zammert and Eckhardt 2014[22]) have been reported.

1.4 Outline of the thesis

The purpose of this study is to understand the transition process to turbulence in plane channel flow. Since it is one of the most common systems in engineering applications, for example used in a heat exchanger, controlling turbulence and realizing high efficiency in channel flow is a significant task. As a first step, we investigate therein the relatively simpler turbulence observed in the transitional regime than that at the high Reynolds number. Identifying the properties of localized turbulence, we describe the growing process. In chapter 2, the direct numerical simulation procedure of plane channel flow and searching methods for invariant solutions are described. In chapter 3, we investigate the dependence of the lifetime on the spanwise extent of the streamwise localized turbulence. Unlike pipe flow whose circumference is fixed at 2π, we can control spatial structures of turbulence by changing the spanwise numerical domain. We expect that the relationship between lifetime and the number of coherent structures can be discussed and the lifetime in the wider case is estimated. In chapter 4, we search a spatially localized edge state by using edge tracking algorithm and Newton-Krylov hookstep iteration. An edge state can be a important solution to explain subcritical transition to turbulence. Obtaining a localized edge state, we attempt to describe the process from a local disturbance to a turbulent spot. In chapter 5, we perform DNS in a large numerical domain and observe a localized turbulent band. Since after growing of a turbulent spot, it shows band-like development, we observe the development of turbulence after the process shown in chapter 4. Then, we identify a sustaining and growing mechanism of a localized turbulent band and generalize the developing process in plane channel flow. Finally, in chapter 6, this thesis is concluded with the summary and future problems.

Chapter 2

Numerical procedure

2.1 Direct numerical simulation

2.1.1 Governing equations

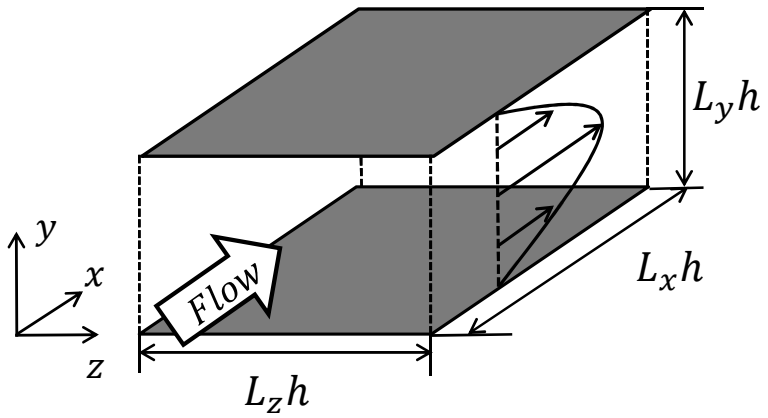

Figure 2.1: Computational domain of plane channel flow

We consider the incompressible flow driven by an external force between two parallel plates separated by the distance of $2h$. We also impose the constant bulk mean velocity U. The coordinate x, y and z are taken in the streamwise direction, the wall-normal direction and the spanwise direction, respectively. The computational domain in our study is defined as $[0, L_x h], [-h, h], [0, L_z h]$ with periodic boundary conditions in the streamwise and spanwise directions and no-slip condition at the wall. The schematic view is shown in Figure 2.1. Nondimensionalizing by the channel half distance h and the center-line velocity of laminar flow $U_c = 3U/2$, the incompressible Navier-Stokes equations governing the flow can be written as

$$\nabla \cdot \boldsymbol{u} = 0 \tag{2.1}$$

$$\frac{\partial \boldsymbol{u}}{\partial t} + \boldsymbol{u} \cdot \nabla \boldsymbol{u} = -\nabla p + \frac{1}{Re} \Delta \boldsymbol{u} \tag{2.2}$$

where $\boldsymbol{u} = (u_x, u_y, u_z)$ is the velocity vector, p is the pressure and $Re = hU_c/\nu$ (ν being kinematic viscosity) is the Reynolds number. The corresponding value defined by mass flux is $Re_m = hU/\nu = 3Re/2$. The vorticity vector is taken to be $\boldsymbol{\omega} = (\omega_x, \omega_y, \omega_z) = \nabla \times \boldsymbol{u}$.

We numerically solve the equivalent equations to (2.2) about the wall-normal component of velocity and vorticity and the x-z averaged streamwise and spanwise velocity defined as

$$\langle u_x \rangle_{xz} = \frac{1}{L_x L_z} \int_0^{L_x} \int_0^{L_z} u_x \mathrm{d}x\mathrm{d}z \tag{2.3}$$

$$\langle u_z \rangle_{xz} = \frac{1}{L_x L_z} \int_0^{L_x} \int_0^{L_z} u_z \mathrm{d}x\mathrm{d}z, \tag{2.4}$$

which are given by

$$\frac{\partial \Delta u_y}{\partial t} = -\left(\nabla \times (\nabla \times (\boldsymbol{u} \times \boldsymbol{\omega}))\right)_y + \frac{1}{Re}\left(\Delta^2 u_y\right) \tag{2.5}$$

$$\frac{\partial \omega_y}{\partial t} = \left(\nabla \times (\boldsymbol{u} \times \boldsymbol{\omega})\right)_y + \frac{1}{Re}\Delta \omega_y \tag{2.6}$$

$$\frac{\partial}{\partial t}\frac{\partial^2 \phi_x}{\partial y^2} = \frac{\partial}{\partial y}\left\langle (\boldsymbol{u} \times \boldsymbol{\omega})_x \right\rangle_{xz} + \frac{1}{Re}\frac{\partial^4 \phi_x}{\partial y^4} \tag{2.7}$$

$$\frac{\partial}{\partial t}\frac{\partial^2 \phi_z}{\partial y^2} = \frac{\partial}{\partial y}\left\langle (\boldsymbol{u} \times \boldsymbol{\omega})_z \right\rangle_{xz} + \frac{1}{Re}\frac{\partial^4 \phi_z}{\partial y^4}, \tag{2.8}$$

where (ϕ_x, ϕ_z) is defined by

$$\frac{\partial \phi_x}{\partial y} = \langle u_x \rangle_{xz}, \frac{\partial \phi_z}{\partial y} = \langle u_z \rangle_{xz}. \tag{2.9}$$

Then, boundary conditions at $y = \pm 1$ are given by

$$u_y = \omega_y = \frac{\partial u_y}{\partial y} = \frac{\partial \phi_x}{\partial y} = \frac{\partial \phi_z}{\partial y} = 0. \tag{2.10}$$

2.1.2 Numerical integration

We discretize (2.5)-(2.8) under the boundary condition (2.10) and carry out the numerical integration. In the spatial discretization, we perform the spectrum expansion by using the Chebyshev-Galerkin method. The Fourier expansions are employed in the streamwise and spanwise directions and the Chebyshev-polynormal expansion in the wall-normal direction. Boundary conditions at the wall are treated by the Galerkin method. $\boldsymbol{u} = (u_x, u_y, u_z)$ and ω_y are expanded as,

$$\boldsymbol{u} = \sum_{j=-J}^{J} \sum_{k=0}^{K-4} \sum_{m=-M}^{M} \hat{\boldsymbol{u}}_{jkm} \left(T_k - \frac{2(k+2)}{k+3} T_{k+2} + \frac{k+1}{k+3} T_{k+4}\right) \exp\left\{\mathrm{i}\left(\frac{2\pi}{L_x} jx + \frac{2\pi}{L_z} mz\right)\right\} \tag{2.11}$$

$$\omega_y = \sum_{j=-J}^{J} \sum_{k=0}^{K-2} \sum_{m=-M}^{M} \hat{\omega}_{jkm} \left(T_k - T_{k+2}\right) \exp\left\{\mathrm{i}\left(\frac{2\pi}{L_x} jx + \frac{2\pi}{L_z} mz\right)\right\}, \tag{2.12}$$

where (j, k, m) represent the wave number in each directions and (J, K, M) are the maximum orders for truncations. $T_k(y)$ indicates the Chebyshev polynominal which has following expression,

$$T_k(y) = \cos(kl), y = \cos l. \tag{2.13}$$

Time stepping is performed with the second-order Adams-Bashforth scheme for the nonlinear terms and the Crank-Nicholson scheme for the viscous terms.

2.2 Edge tracking

In plane channel flow, while the laminar state becomes unstable at a critical value of Reynolds number $Re_c \simeq 5772$[23], a turbulent state realizes even at lower Reynolds number $Re < Re_c$. That means that the transition to turbulence is more or less the same as pipe flow and plane Couette flow where the state of the flow is attracted to one of two attractors depending on disturbance amplitude: the trivial laminar state or the turbulent state. The basin boundary of these attractors can be characterized by an invariant solution, i.e. an edge state.

An edge state has only one unstable direction. An edge state and its stable manifold, therefore, can form exactly the basin boundary between laminar and turbulent attractors. The unstable manifold, on the other hand, can indicate the path which leads to these states. That is, a subcritical transition to turbulence can be described as the following scenario. Assuming that a finite amplitude disturbance near the critical amplitude is introduced in the laminar state, the flow state is attracted to the invariant state along the stable manifold of the edge state. As long as it is not on a stable manifold, the flow state eventually attains the laminar or turbulent state. The process of developing or decay can be characterized by an unstable manifold. In other words, investigating the feature of the edge state has an great importance to explain the subcritical transition to turbulence.

In order to obtain the edge state, we employ the edge tracking algorithm[13, 24]. We define the state finally attracted to the turbulent attractor as $\boldsymbol{u}_t$ and the state which will approach the laminar state as $\boldsymbol{u}_l$. Using these states as initial conditions, we define a new initial condition $\boldsymbol{u}^*$ as

$$\boldsymbol{u}^* = (1 - \lambda)\boldsymbol{u}_l + \lambda \boldsymbol{u}_t, \tag{2.14}$$

where λ $(0 \leq \lambda \leq 1)$ is a parameter in the linear combination, and $\boldsymbol{u}^* = \boldsymbol{u}_t$ when $\lambda = 1$ and $\boldsymbol{u}^* = \boldsymbol{u}_l$ when $\lambda = 0$. We tune λ so that, $\boldsymbol{u}^*$ may lead to a trajectory that follows the stable manifold of the edge state. We can specify the edge state by updating the initial condition and repeating this bisection. Figure 2.2 shows a schematic view.

Carrying out the edge tracking, the flow state is evaluated by the energy E_{3d} of the fluctuation component from the laminar flow,

$$E_{3d} = \frac{1}{4L_xL_z} \int_V \left\{ (u_x - U_{LF})^2 + u_y^2 + u_z^2 \right\} dV \tag{2.15}$$

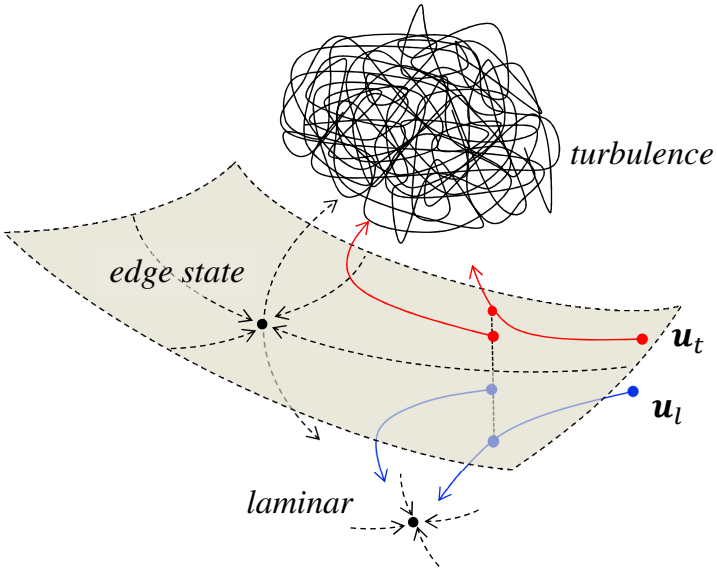

Figure 2.2: Edge tracking

where the laminar solution is defined as $U_{LF}(y) = 1 - y^2$. E_{3d} getting larger, the state becomes the turbulence and $E_{3d} = 0$ shows the laminar flow. Employing the edge tracking, we evaluate the turbulent or laminar consequence by setting a certain threshold.

2.3 Newton iteration

Searching the unstable periodic orbit embedded the turbulent state, we perform the Newton-Krylov iteration. Unlike the edge tracking, we can obtain the invariant solution which has more than one unstable directions. Following Viswanath (2007)[25], the procedure searching the unstable periodic orbit is described as below.

We consider an N-dimensional dynamical system defined as

$$\frac{dX_i}{dt} = f_i(\boldsymbol{X}), \tag{2.16}$$

where $\boldsymbol{X} = (X_1, X_2, \ldots, X_N)$ represents a state point in an N-dimensional phase space and $\boldsymbol{f} = (f_1, f_2, \ldots, f_N)$ is a vector field defined by a certain function (incompressible Navier-Stokes equations in this study). The variables which determine the state of the flow are given by $\hat{\boldsymbol{u}}_{jkm}, \hat{\omega}_{jkm}$. In fact, the dimension in phase space N is equivalent to the number of all the variables.

Now we consider searching a periodic orbit of a dynamical system (2.16). In order to obtain the periodic motion, we have to introduce the period of orbit T. Further, we also consider that the turbulent structure is advected downstream in plane channel flow. Hence, it is necessary to match the phases of the initial state and the state after the period T. In this case, our target is a relative periodic

orbit. Considering the no phase shift in the wall-normal direction, we define s_x and s_z as the streamwise phase shift and the spanwise phase shift, respectively. Therefore, we describe the Newton method considering T, s_x and s_z in addition to the N variables below.

Let $\boldsymbol{X}(\boldsymbol{X}_0; T)$ be the state point after time evolution T from the initial condition point $\boldsymbol{X}_0$. (2.11) and (2.12) undergoing the phase shift s_x and s_z are given by

$$\begin{pmatrix} u_y(x+s_x, y, z+s_z) \\ \omega_y(x+s_x, y, z+s_z) \end{pmatrix} = \sum_{j=-J}^{J} \sum_{m=-M}^{M} A \begin{pmatrix} \tilde{u}_{jm}(y) \\ \tilde{\omega}_{jm}(y) \end{pmatrix} \exp\left\{ \mathrm{i}\left(\frac{2\pi}{L_x} jx + \frac{2\pi}{L_z} mz \right) \right\} \tag{2.17}$$

$$A = \exp\left(\mathrm{i}\frac{2\pi}{L_x} j s_x \right) \exp\left(\mathrm{i}\frac{2\pi}{L_z} m s_z \right) \tag{2.18}$$

where the streamwise and spanwise velocity component u_x and u_z are omitted because of x-z average. Following Viswanath (2007)[25] we introduce the differential operator $\mathcal{T}_1$ and $\mathcal{T}_2$ as

$$\mathcal{T}_1 \begin{pmatrix} u_y(x,y,z) \\ \omega_y(x,y,z) \end{pmatrix} = \sum_{j=-J}^{J} \sum_{m=-M}^{M} \left(\mathrm{i}\frac{2\pi}{L_x} j \right) \begin{pmatrix} \tilde{u}_{jm}(y) \\ \tilde{\omega}_{jm}(y) \end{pmatrix} \exp\left\{ \mathrm{i}\left(\frac{2\pi}{L_x} jx + \frac{2\pi}{L_z} mz \right) \right\} \tag{2.19}$$

$$\mathcal{T}_2 \begin{pmatrix} u_y(x,y,z) \\ \omega_y(x,y,z) \end{pmatrix} = \sum_{j=-J}^{J} \sum_{m=-M}^{M} \left(\mathrm{i}\frac{2\pi}{L_z} m \right) \begin{pmatrix} \tilde{u}_{jm}(y) \\ \tilde{\omega}_{jm}(y) \end{pmatrix} \exp\left\{ \mathrm{i}\left(\frac{2\pi}{L_x} jx + \frac{2\pi}{L_z} mz \right) \right\}, \tag{2.20}$$

where (2.17) can be replaced by using $\mathcal{T}_1$ and $\mathcal{T}_2$ as $\exp(s_x\mathcal{T}_1)\exp(s_z\mathcal{T}_2)(u_y, \omega_y)^t$. Therefore, applying $\boldsymbol{X}_0$, it becomes $\exp(s_x\mathcal{T}_1)\exp(s_z\mathcal{T}_2)\boldsymbol{X}_0$. Now, according to the space translation invariance for the Navier-Stokes equations, following relationship is established.

$$\boldsymbol{f}(\exp(s_x\mathcal{T}_1)\exp(s_z\mathcal{T}_2)\boldsymbol{X}) = \exp(s_x\mathcal{T}_1)\exp(s_z\mathcal{T}_2)\boldsymbol{f}(\boldsymbol{X}) \tag{2.21}$$

Based on above, searching a relative periodic orbit in plane channel flow, we determine $\boldsymbol{X}^*, s_x, s_z$ and T that satisfy

$$\exp(s_x\mathcal{T}_1)\exp(s_z\mathcal{T}_2)\boldsymbol{X}(\boldsymbol{X}^*; T) = \boldsymbol{X}^*. \tag{2.22}$$

First, we determine $\boldsymbol{X}_0, s_x, s_z$ and T as initial guesses and calculate $\boldsymbol{Y}_0$ defined as $\boldsymbol{Y}_0 = \exp(s_x\mathcal{T}_1)\exp(s_z\mathcal{T}_2)\boldsymbol{X}(\boldsymbol{X}_0; T)$. Linearizing (2.22) we obtain following equations,

$$\begin{pmatrix} \exp(s_x\mathcal{T}_1)\exp(s_z\mathcal{T}_2)\dfrac{\partial \boldsymbol{X}(\boldsymbol{X}_0;T)}{\partial \boldsymbol{X}_0} - I & \mathcal{T}_1\boldsymbol{Y}_0 & \mathcal{T}_2\boldsymbol{Y}_0 & \boldsymbol{f}(\boldsymbol{Y}_0) \\ (\mathcal{T}_1\boldsymbol{X}_0)^t & 0 & 0 & 0 \\ (\mathcal{T}_2\boldsymbol{X}_0)^t & 0 & 0 & 0 \\ (\boldsymbol{f}(\boldsymbol{X}_0))^t & 0 & 0 & 0 \end{pmatrix} \begin{pmatrix} \delta\boldsymbol{X}_0 \\ \delta s_x \\ \delta s_z \\ \delta T \end{pmatrix} = \begin{pmatrix} \boldsymbol{X}_0 - \boldsymbol{Y}_0 \\ 0 \\ 0 \\ 0 \end{pmatrix}, \tag{2.23}$$

where I is the identity matrix and $\delta\boldsymbol{X}_0, \delta s_x, \delta s_z$ and δT are the correction amounts. After solving (2.23) and determining $\delta\boldsymbol{X}_0, \delta s_x, \delta s_z$ and δT, initial guesses are updated to $\boldsymbol{X}_0 + \delta\boldsymbol{X}_0, s_x + \delta s_x, s_z + \delta s_z$ and $T + \delta T$. We iterate these procedure until

following convergence condition

$$\frac{\|\boldsymbol{Y}_0 - \boldsymbol{X}_0\|}{\|\boldsymbol{X}_0\|} < 10^{-10} \tag{2.24}$$

is satisfied. Now we solve (2.23) and determine the correction amount $\delta\boldsymbol{X}_0$, δs_x, δs_z and δT. If the degrees of freedom N is huge as in our dynamical system, it cannot be solved due to insufficient memory of the computer. Therefore, we use the GMRES (generalized minimal residual method) iteration to solve (2.23) approximately. The combined method using Newton iteration and GMRES is called the Newton-Krylov iteration which is employed to search an unstable invariant solution embedded in the turbulent motion (see Sanchesz *et al.*[26] and Viswanath[25]).

In order to converge the solution by using the Newton iteration, choosing a good initial estimate has a great importance. If the initial condition is far from the solution, it will not converge and and thus the calculation may fail. Therefore, we employ the hookstep method [27] to improve the global convergence of the Newton-Krylov iteration. By using the combined Newton-Krylov hookstep iteration, Brand and Gibson (2014)[21] have obtained the spatially-localized solution in the streamwise and spanwise directions in plane Couette flow and hence it can also be a useful procedure in our study.

Chapter 3

Exponential growth of lifetime of localized turbulence with its extent in channel flow

3.1 Introduction

Laminar velocity profiles in pipe flow and plane Couette flow are linearly stable at any Reynolds number, see Salwen *et al.* (1980)[28] for pipe flow and Romanov (1973)[29] for plane Couette flow. In plane channel flow, although it becomes linearly unstable at finite Reynolds number, transition to turbulence can be promoted by sufficiently large disturbances even at much lower Reynolds number. In these systems, therefore, it is difficult to identify the route to turbulence as the result of a series of linear instabilities, and it has long been an open question. One of the most critical breakthrough for this problem is the discovery of lifetime of turbulence (Schmiegel and Echhardt 1997[30] and Bottin *et al.* 1998[31] for plane Couette flow; Faisst and Eckhardt 2004[32], Hof *et al.* 2006[33], Peixinho and Mullin 2006[34] and Willis and Kerswell 2007[35] for pipe flow). Flow at the Reynolds number for which transient turbulence can be observed is called transitional. In transitional flow, spatially localized turbulence exists and decays suddenly to laminar flow after transient. Localized turbulence has been observed as puffs in pipes (Wygnansky and Champagne 1973[2]) and its lifetime thoroughly investigated. In dynamical systems terminology, transient turbulence is attributed to the presence of chaotic saddles out of which chaos decays according to exponentially decaying distributions of lifetimes (Faisst and Eckhardt 2004[32]). The most recent consensus is about a double-exponential increase of mean lifetimes with the Reynolds number (Hof *et al.* 2008[11]; Avila *et al.* 2011[3]), interpreted within the framework of extreme value theory by Goldenfeld *et al.* (2010). Although their lifetimes are not for localized turbulence, Schneider and Eckhardt (2008)[36] reported the exponential dependence of turbulence lifetimes on the pipe length.

In plane Couette flow and plane channel flow, transitional flow is initiated by localized turbulence in two directions, both the streamwise and spanwise directions, which is called a turbulent spot, see Cantwell *et al.* (1979)[37] for a boundary

layer, Carlson *et al.* (1982)[7] for plane channel flow and Tillmark and Alfredsson (1992)[38] for plane Couete flow. At slightly higher Reynolds number, band patterns of turbulence can also be observed (Prigent *et al.* 2003[39]; Tsukahara *et al.* 2005[8]). Although such band turbulence, which is elongated in one direction, might possibly be transient below some critical Reynolds number (Manneville 2011[10]; Shi *et al.* 2013[40]; Xiong *et al.* 2015[41]), there is no detailed measurement of lifetimes in two-dimensionally extended system. This is because the effect of its spanwise extent causes the problem more complex than one-dimensionally extended system like pipe flow. In plane Couette flow, a turbulent band decays abruptly followed by a large laminar gap, which can be regarded as large deviations of an underlying stochastic process (Manneville 2011[10]). Typically the size of the gap along the band which leads to decay is $O(10h)$, h being half the distance between the two walls. In this chapter we investigate the dependence of lifetimes both on the Reynolds number and the spanwise extent using streamwise-localized turbulence in plane channel flow. This dependence might relate to the probability distribution of laminar gaps in turbulent bands in an extended system.

3.2 Numerical settings

The streamwise period is set to $L_x = 100$, and this length may be considered to be sufficient for a single turbulent 'puff'. We vary the the aspect ratio, which is defined as $A = L_z/2$, in the range of $0.5 \leq A \leq 5$. Hereafter we use A as the parameter of spanwise length. Although the short period in the z direction is unrealistic, in this artificial system we can investigate the influence of the spanwise extent of the turbulent puff on its lifetime. The maximum wavenumbers in the x and z directions and the maximum order of polynomials in the y direction are set to $(533, 47, [(64A - 1)/3])$, where $[\cdot]$ means the integer part of the number. Computational settings are summarized in table 3.1.

Table 3.1: Computational conditions

Aspect ratio A	Truncation degree (J, K, M)	Initial condition Re_m
0.50	$(533, 47, 10)$	1400
0.75	$(533, 47, 15)$	1126.7
1.00	$(533, 47, 21)$	1050
1.25	$(533, 47, 26)$	1010
1.50	$(533, 47, 31)$	950
2.50	$(533, 47, 53)$	926.7
5.00	$(533, 47, 106)$	818.7

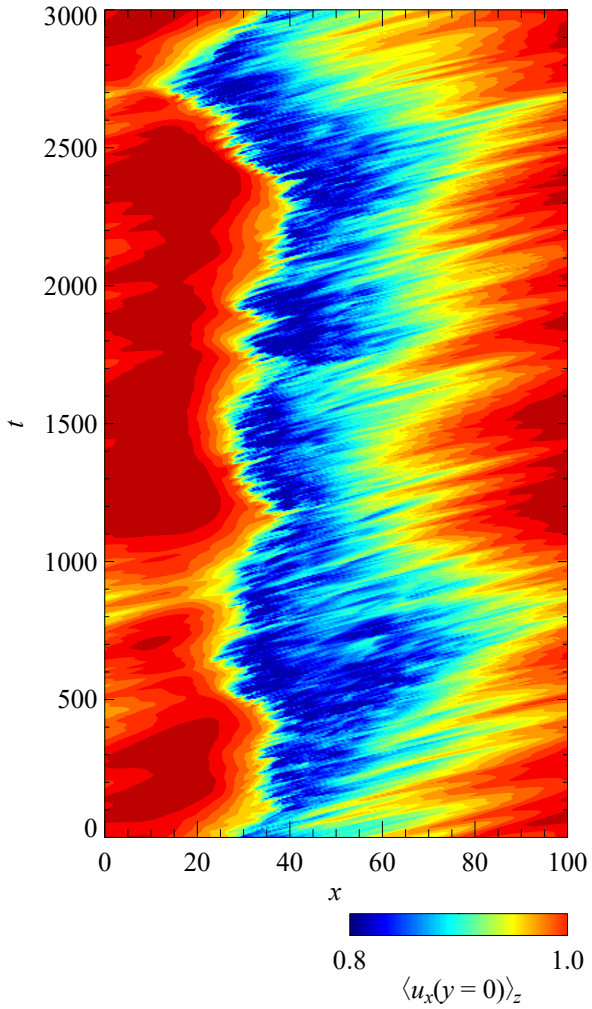

Figure 3.1: Time series of the spanwise-averaged streamwise velocity u_x on the mid-plane $y = 0$ for $A = 1.5$ and at $Re_m = 1010$.

3.3 Lifetime

We investigate the dependence of lifetime of the turbulent puff on Re_m and A. The lifetime is defined as wandering duration close to chaotic invariant sets in phase space before decaying to the laminar state, which is the unique stable solution at Re in our survey. As initial conditions we prepare many turbulent puffs at different Re_m. If some of the orbits from these initial conditions are trapped around some wandering state, we can estimate the characteristic time scale to escape from it, the lifetime τ. For example, at $Re_m = 1000$ and for $A = 1.25$ we show how the lifetime is estimated. Figure 3.1 shows the streamwise and temporal variation of the streamwise velocity u_x averaged over the spanwise direction on the mid-plane $y = 0$ at $Re_m = 1010$. The horizontal axis represents the x axis of the reference frame moving at the puff's velocity U_p. The region in which velocity is close to 1 is laminar and the low-speed region represents the turbulent puff. Every time interval 5 the total 512 velocity fields at $Re_m = 1010$ are taken as a set of initial

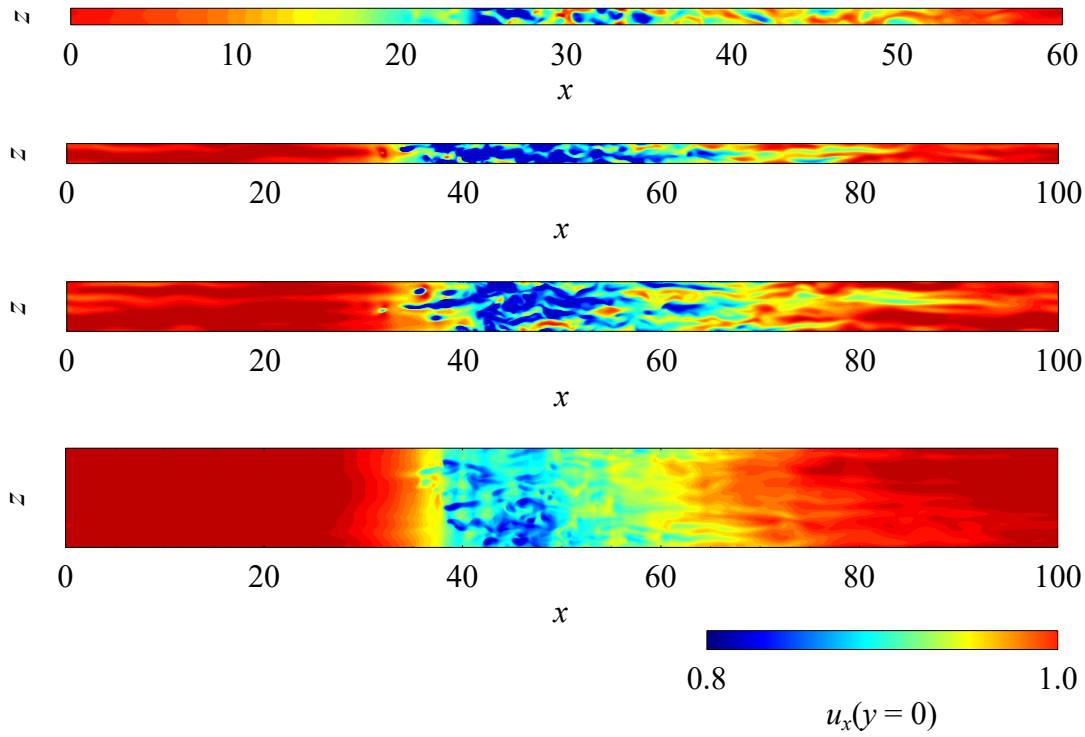

Figure 3.2: Spatial distribution of the streamwise velocity u_x on the mid-plane $y = 0$ for various aspect ratio A. $A = 0.5(Re_m = 1400), 1(Re_m = 1050), 2.5(Re_m = 926.7)$ and $5(Re_m = 818.7)$ from the top.

conditions to estimate the lifetime at $Re_m = 1000$. In figure 3.2 snapshots of localized turbulence for several aspect ratios are shown. Because the period in the spanwise direction is small for these aspect ratios the localized structures are fully extended in this direction. The localized turbulence in this system resembles a turbulent puff in pipe flow in the sense that it exhibits one-dimensional localization, and thus we have referred to it as a turbulent 'puff'. Figure 3.3 shows time series of skin friction from 40 initial conditions. Turbulent puffs are regarded to be 'dead' when the skin friction $d = \left\langle |du_x/dy|_{x=\pm 1} \right\rangle /3$ (where $\langle \cdot \rangle$ denotes averaging over the walls), is smaller than 1.05, 1 corresponding to laminar flow.

We measure the lifetime of each turbulent puff and investigate the time dependence of the survival probability. Figure 3.4 shows probability distributions of lifetime $P(t)$ at several Reynolds numbers for $0.50 \leq A \leq 5.00$. $P(t)$ means the ratio of survivors at $t - t_0$ in 512 samples, where t_0 is the shortest lifetime at the considered Reynolds number.

The duration of simulations at each Reynolds number is $t_c = 500$. Distributions of lifetime are supposed to be exponential, $P(t) = \exp(-(t-t_0)/\tau)$. The maximum likelihood estimate for mean lifetimes τ for censored data, Type 2 censoring in Lawless (2011)[42], are given by

$$\hat{\tau} = \frac{1}{r} \left\{ \sum_{i=1}^{r} (t_i - t_0) + (n - r)(t_r - t_0) \right\}, \tag{3.1}$$

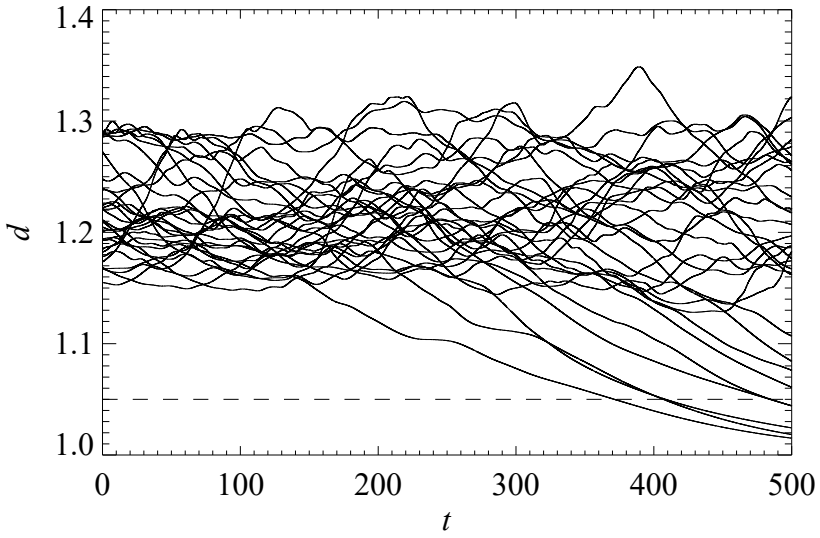

Figure 3.3: Temporal evolution from 40 different initial conditions for $A = 1.5$ and $Re_m = 1000$. The dashed line represents the threshold of relaminarization.

where $n = 512$ is the number of samples and t_i $(i = 1, 2, \ldots, r)$ are r smallest lifetimes observed until t_c, $t_0 < t_1 < t_2 < \cdots < t_r < t_c$. Dotted lines in figure 3.4 represent the fitting functions $P(t) = \exp(-(t - t_0)/\hat{\tau})$. The dependence of estimated lifetimes $\hat{\tau}$ on the Reynolds number and the aspect ratio is plotted in figure 3.5. The lifetime is a monotonically increasing function of the Reynolds number and the aspect ratio. The dependence on the Reynolds number is well fitted by the double-exponential model $\exp\{\exp(aRe_m + b)\}$, (Avila *et al.* 2011[3]; Goldenfeld *et al.* 2010[43]). Dashed lines in the figure represent the fitted function using the least squared method to determine two parameters, a and b. In the following we investigate the dependence on the aspect ratio.

Consider independent and identical turbulence sites which stand side by side in the spanwise direction. They may be regarded as the minimal flow unit accommodating one low-speed streak associated with streamwise vortices (Jiménez and Moin 1991[44]). Turbulence decays when all the sites decay at the same time. If the lifetime of the site equals to be τ_0, the lifetime of a turbulent puff, which has N sites inside itself in the spanwise direction, becomes τ_0^N. If we suppose that N is proportional to the aspect ratio A, then

$$\ln(\tau) \propto A. \tag{3.2}$$

Figure 3.6 shows the dependence of lifetimes on the aspect ratio at $Re_m = 800, 900$ and 1000. As the aspect ratio increases τ increases and $\ln(\tau)$ seems to be proportional to A for relatively small A. The dashed lines are fitting functions by equation 3.2 using only in the range of $0.75 \leq A \leq 1.7$. The factor of proportionality increases as the Reynolds number increases. For large A lifetime increases more slowly than exponentially with increasing A. This may be the consequence of spanwise-localization effect for larger A and at smaller Re_m. Note that lifetime for $A = 0.5$ in figure 3.5 is obviously smaller than expected values from equation

(*a*)

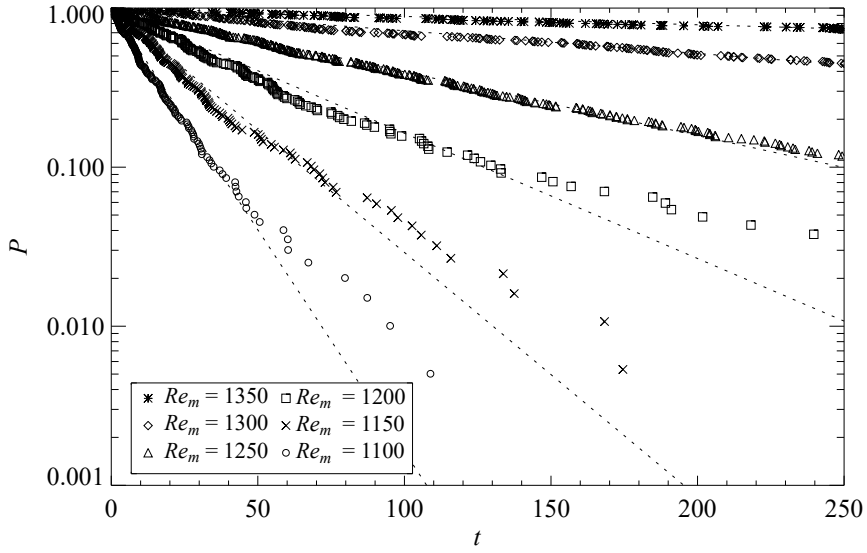

(*b*)

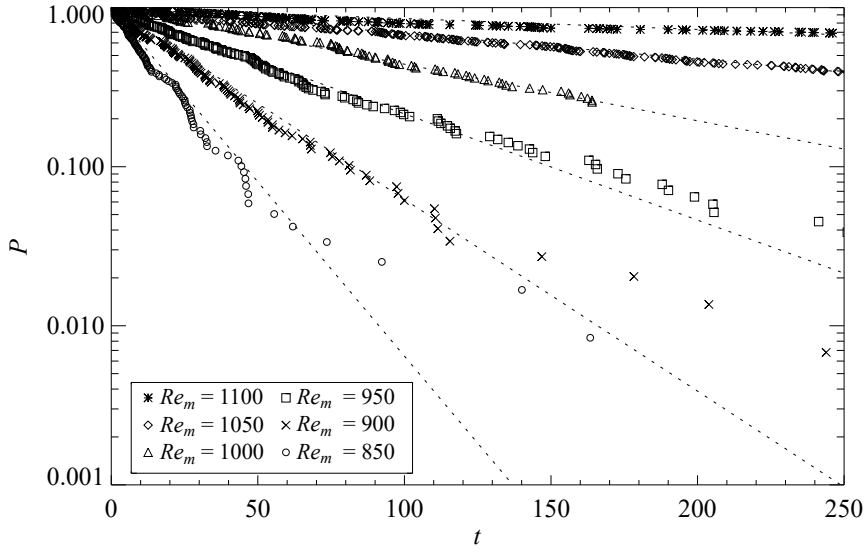

Figure 3.4: Probability distribution at several Reynolds numbers Re_m. (*a*) $A = 0.50$, (*b*) $A = 0.75$, (*c*) $A = 1.00$, (*d*) $A = 1.25$, (*e*) $A = 1.50$, (*f*) $A = 2.50$, (*g*) $A = 5.00$. The dashed lines represent $P(t) = \exp\{-(t - t_0)/\tau\}$, where τ is defined by (3.1).

(*c*)

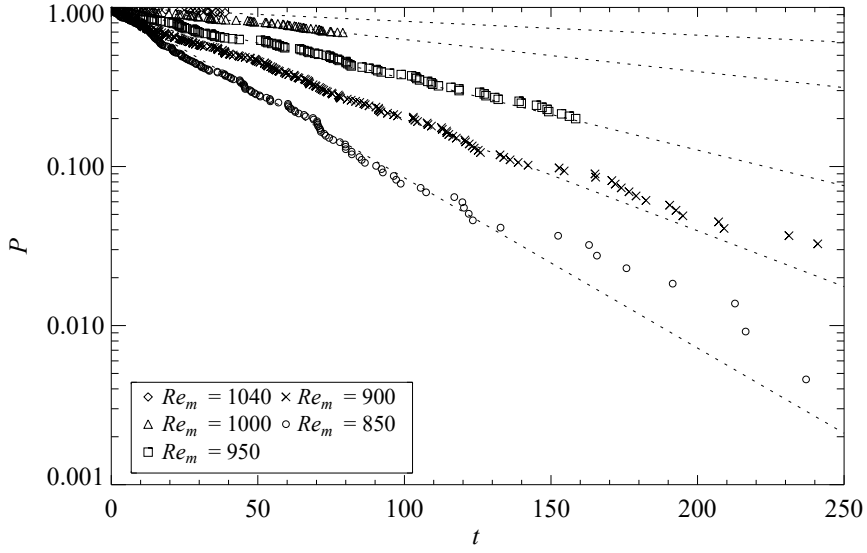

(*d*)

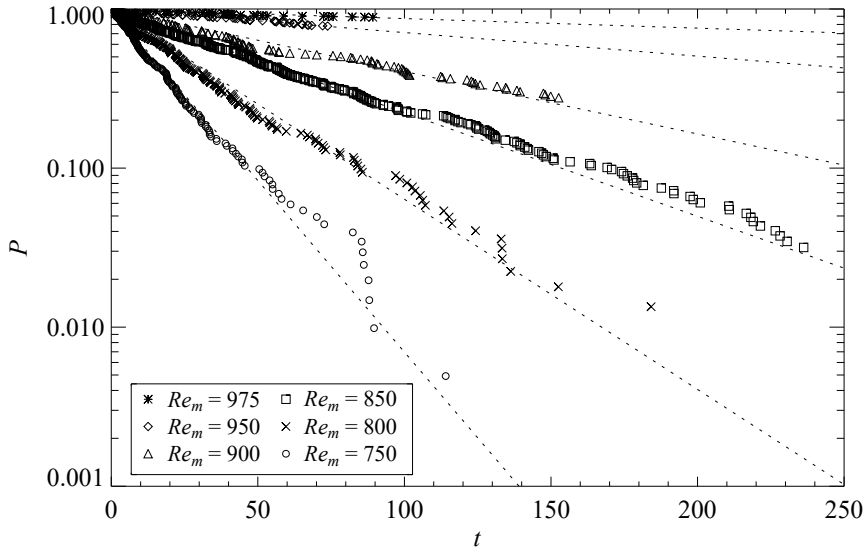

Figure 3.4: Continued.

(e)

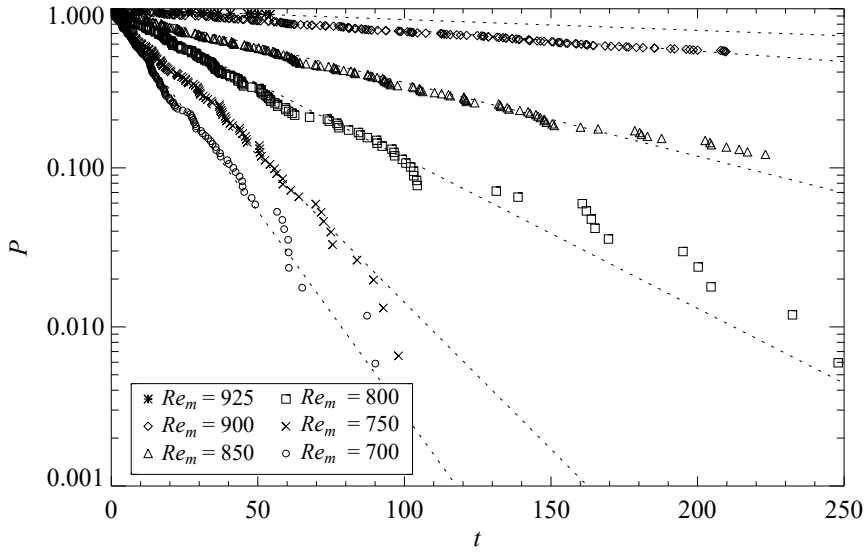

(f)

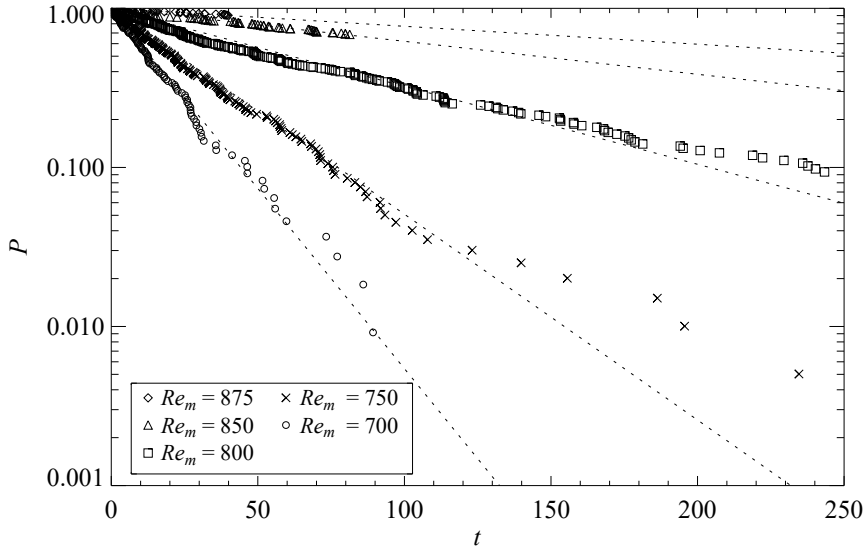

Figure 3.4: Continued.

(g)

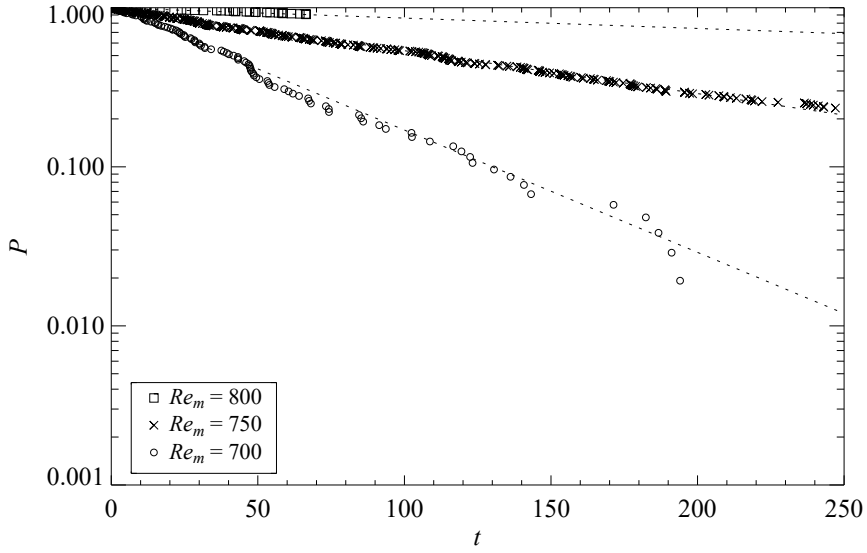

Figure 3.4: Continued.

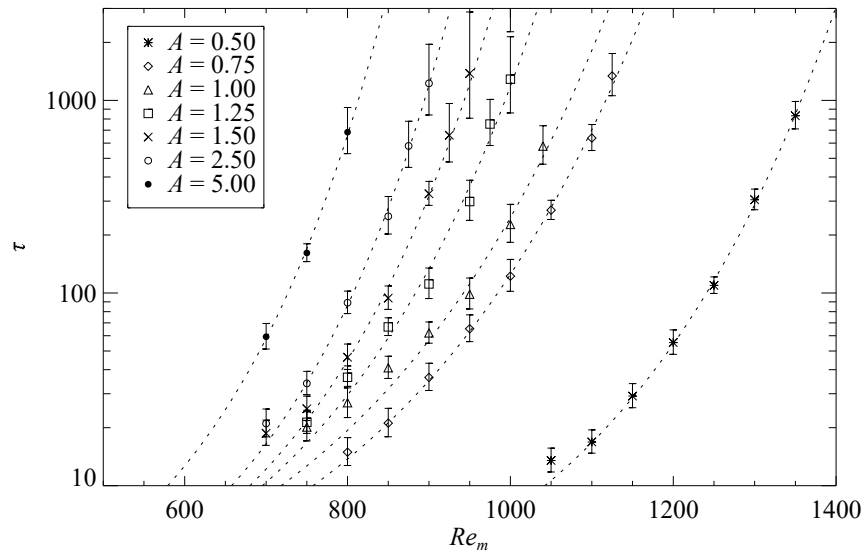

Figure 3.5: Mean lifetime of localized turbulence for each aspect ratio A. The erorr bars indecate 95 % confidental intervals . The dashed lines are given by the superexponential function $\tau = \exp\{\exp(aRe_m + b)\}$, where a and b are fitting parameters.

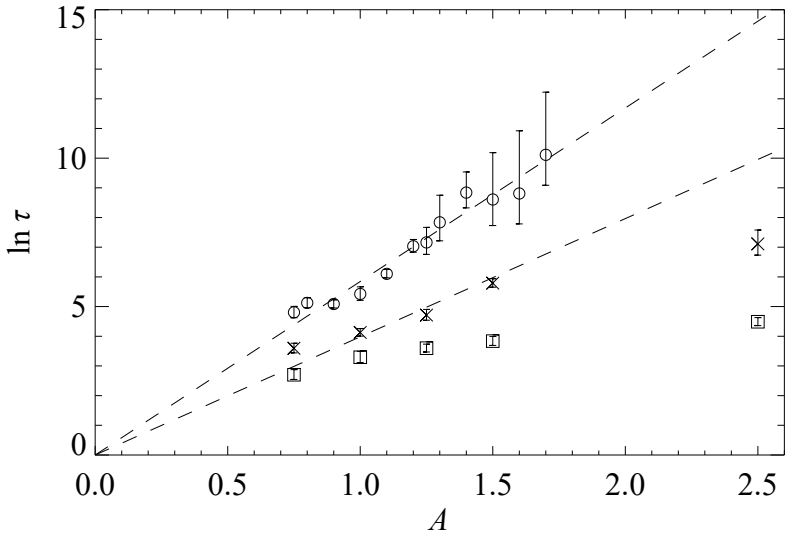

Figure 3.6: Plots of logarithm of lifetime, $\ln(\tau)$, for several aspect ratios A at $Re_m = 800(\square), 900(\times)$ and $1000(\circ)$. The dashed lines represent the fitting functions $\ln\tau = 5.8A$ and $\ln\tau = 4.0A$ from the top.

3.2. This may relate to observation that turbulence exists only on one wall for $A = 0.5$. Typically the spanwise spacing of low-speed streaks around the training edge of a puff is about 1 at $Re_m = 1000$; e.g. there are two low-spead streaks for $A = 1$. It seems that τ does not change much around $A = 0.8$ and $A = 1.5$. This stepwise increase of τ may correspond to discrete change of the number of low-spead streaks.

3.4 Concluding remarks

We investigated the dependence of the lifetime on the spanwise extent of the turbulent puff. For moderate spanwise extent, the lifetime increases exponentially as a function of the aspect ratio. This can be considered to be a consequence of near i.i.d (independent and identically distributed) property of turbulent structures.

Figure 3.7 shows the probability density function (PDF) of maximum of $(U_{LF} - u_x)|_{y=\pm 0.8}$ at $Re_m = 1050, 1060$ and 1070 and for $A = 1$. These maximum values correspond to the strongest low-speed streak at each moment. This PDF is close to a Gumbel distribution and does not depend much on Re_m, although the range of Re_m is not so large. By fitting the PDF to the Gumbel distribution the Gumbel parameters can be estimated as $\mu \simeq 0.125$ and $\beta \simeq 0.016$ for these Re_m. From the model of lifetime in Goldenfeld *et al.* (2010)[43],

$$\begin{aligned} \mathrm{lnln}(\tau/\tau_0) &= -(B_c - \mu)/\beta & (3.3)\\ &\simeq -\{B_c^0 + B_c^1(Re_m - Re_{m0}) - \mu\}/\beta, & (3.4) \end{aligned}$$

where τ_0 is the correlation time, for which we can regard trials are independent, and B_c is the threshold above which turbulence can sustain, and B_c^0, B_c^1 are coefficients

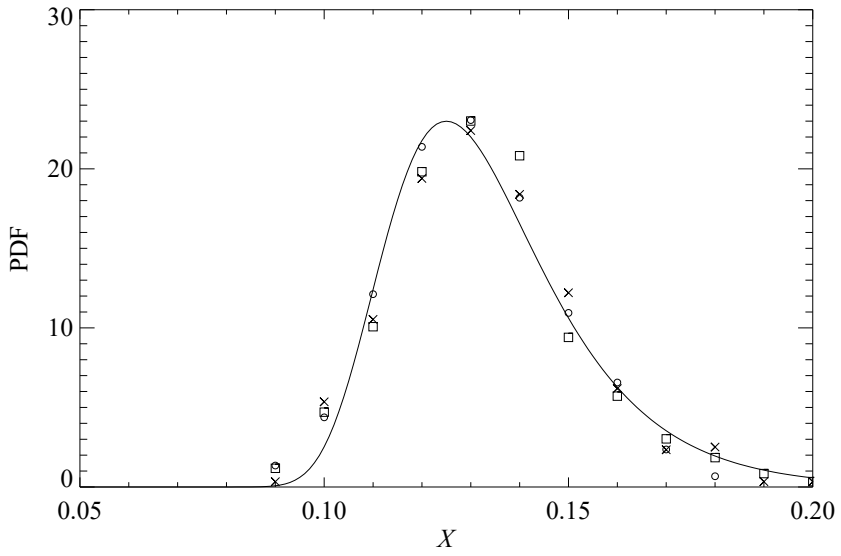

Figure 3.7: Probability distribution function of maximum values of $U_{LF} - u_x$ on the plane $y = \pm 0.8$, X , at $Re_m = 1050(\square), 1060(\times)$ and 1070 $(\circ)$ and for $A = 1$. The solid line represents the Gumbel distribution $\frac{1}{\beta}\exp[-(X-\mu)/\beta]\exp\{\exp[-(X-\mu)/\beta]\}$, where $\mu = 0.125$ and $\beta = 0.016$.

of the Taylor expansion around $Re_m = Re_{m0}$. Here we can take $\tau(Re_{m0}) = e\tau_0$ then $B_c^0 = \mu$. Figure 3.8 represents the dependence of the coefficient a and b in the expression as $\tau = \exp[\exp[aRe_m + b]]$. For $\tau \gg \tau_0$ these coefficients are $a = -B_c^1/\beta, b = B_c^1 Re_{m0}/\beta$. In the case of $A = 1$ the dependence of the threshold B_c on Re_m is estimated as $B_c = \mu - \beta(aRe_m + b) \simeq 0.15 - 4.8 \times 10^{-5} Re_m$. Because $B_c \simeq 0.1$ at $Re_m = 1050$ the Gumbel's cumulative probability below the threshold B_c becomes $P(B_c) = \exp[-\exp[-(B_c - \mu)/\beta]] \sim 0.01$. If we set the correlation time $\tau_0 \sim 10$, which may correspond to the typical timescale of the self suntanning cycle of a low-speed streak, the average lifetime can be estimated as $\tau = \tau_0/P(B_c) \sim 1000$, and this value is consistent with the observed lifetime from figure 3.5. Although the dynamics of a turbulent puff is determined by a large number of degrees freedom, we can roughly estimate the threshold to decay by using the above extreme value theory.

Our result shows that if the extent of turbulence in the spanwise direction is small enough, its lifetime increases exponentially as a function of the extent. On the other hand, in the case of a turbulent band state in an extended system, a local laminar gap can trigger decay of a entire band (Manneville 2011[10]). In this case, extension of the system size seems to lead to larger possibility to decay because the probability of such a laminar gap may be proportional to the system size. Our measurement of lifetime may correspond to the probability of these laminar gaps in extended bands.

As the extent of streamwise localized turbulence increases, the lowest limit of the Reynolds number, above which transient turbulence can be seen, decreases. The streamwise localized turbulence cannot sustain for a large aspect ratio at

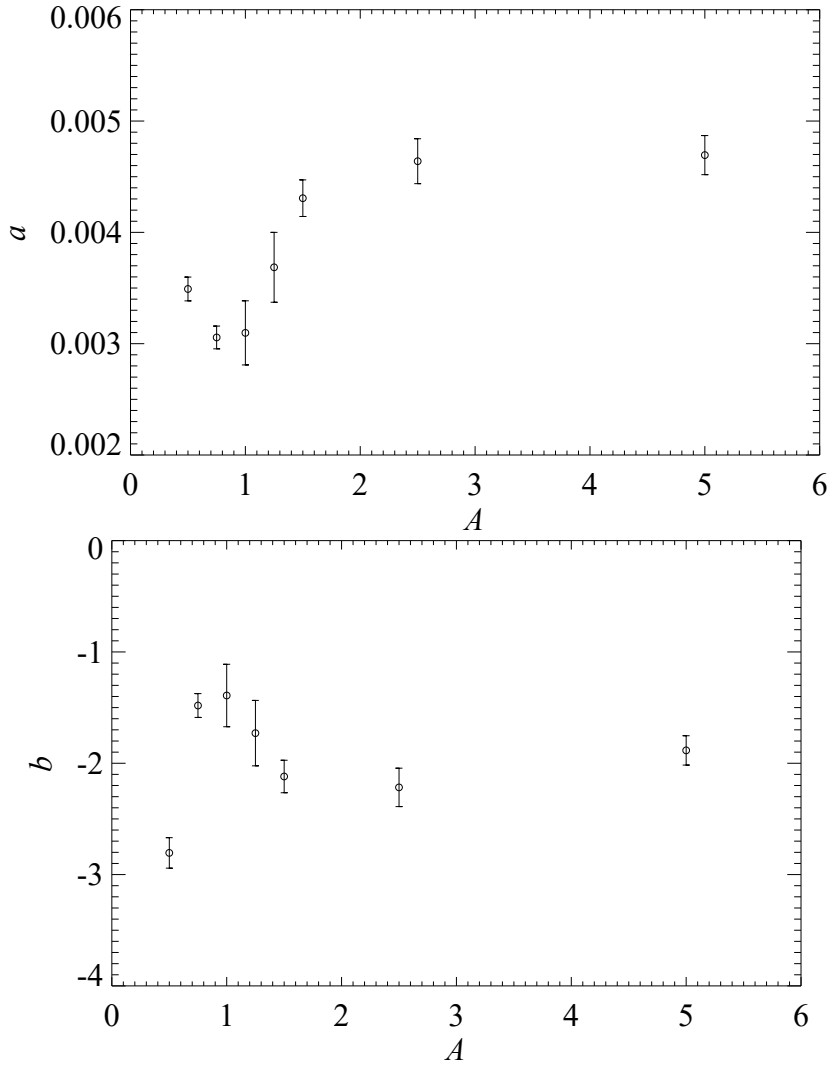

Figure 3.8: The dependence of the fitting coefficients a (top) and b (bottom) on the aspect ratio A in the formula $\tau = \exp[\exp[aRe_m + b]]$.

low Reynolds number. However turbulent bands can be sustained at much lower Reynolds number in an extended system (Xiong *et al.* 2015[41]). Using an oblique domain (Tuckerman and Barkley 2011[9]) direct investigation of the lifetime of turbulent bands is desirable for more quantitative investigation.

Chapter 4

Growing process of localized turbulence in plane channel flow

4.1 Introduction

In plane channel flow, while the laminar profile becomes unstable at a critical value of the Reynolds number (Orszag 1971[23]), turbulence is widely observed at lower Reynolds number. At this range of the Reynolds number, a finite-amplitude disturbance can cause the transition to turbulence which is observed in many other wall-bounded shear flows. In contrast with the gradual change called supercritical transition, the transition to turbulence in plane channel flow and other systems is called subcritical transition. Although the subcritical problem has been long investigated, because of fully nonlinear dynamics its detail have not been clarified yet. In this chapter, we attempt to theoretically describe the subcritical transition to turbulence in plane channel flow. In order to discuss this problem, we investigate an invariant solution called an edge state which can form the basin boundary between laminar and turbulent attractors. The edge state plays an important role to explain the problem of transition to turbulence since it emerges from a saddle-node bifurcation and thus at least in the vicinity of the bifurcation point the saddle solution (referred to as a lower branch) can be an edge state. In plane Couette flow (Kreilos and Eckhard 2012[17]) or pipe flow (Avila *et al.* 2013[20]), a critical Reynolds number at which transient turbulence appears because of a crisis phenomenon on the lower branch solution, i.e. an edge state, is suggested. Furthermore, characteristics of an edge state can play an important role to describe the transition process of a disturbance beyond a critical amplitude. Therefore, investigating this solution is a significant problem (see §2.2.)

The growth of a disturbance beyond a critical amplitude is explained as a development of spatially localized turbulence in plane channel flow. Localized turbulence in the streamwise and spanwise directions is called a turbulent spot which has been observed in the experiment (Alavyoon *et al.* 1986[45]) and numerical simulation (Henningson and Kim 1991[46]). Depending on the Reynolds number, a turbulent spot exhibits the decay to laminar flow or further growth to a turbulent band (Tuckerman *et al.* 2014[47], Xiong *et al.* 2015[41]), however, its formation

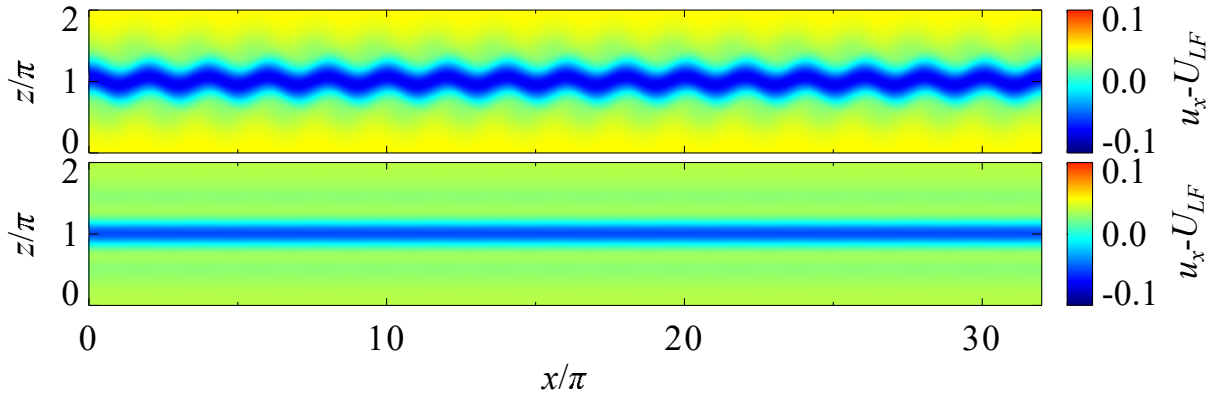

Figure 4.1: Initial condition in the domain of $(L_x, L_z) = (32\pi, 2\pi)$ for $Re = 1400$: (top) mid-plane; (bottom) $y \simeq 0.6$

process of spots is independent of the parameter. In order to theoretically describe it, we investigate a localized edge state in the streamwise and spanwise directions. While a spatially localized invariant solution has been found in plane Couette flow (Brand and Gibson 2014[21]), a localized edge state has not been reported.

In this chapter, we carry out searching a spatially localized edge state. Comparing with the previous report, we will show a new result in §4.2. Next section 4.3, we attempt to describe subcritical transition to turbulence by a stability analysis. In §4.4, we discuss a control of turbulence by adjoint eigenfunction analysis. Then, we conclude this chapter in §4.5.

4.2 Spatially localized edge state

A streamwise localized edge state has been investigated in pipe flow with a spatial symmetry (Avila *et al.* 2013[20]). Also, Zammert and Eckhard (2014)[22] have reported that a streamwise localized edge state in a domain of $(L_x, L_z) = (32\pi, 2\pi)$. Therefore, we investigate this solution and compare with their results.

First, we perform the edge tracking between a turbulent state in $(L_x, L_z) = (2\pi, 2\pi)$ in which the maximum wavenumbers are taken as $(J, K, M) = (10, 47, 15)$ at $Re = 1400$ and the laminar state. However, the trajectory remains a chaotic behavior and it is difficult to converge to an edge state. This is because it takes too long time for the trajectory to follow a stable manifold of an edge state because of the complex state space. So we employ an initial condition in which an invariant solution is periodically connected in the streamwise direction following Zammert & Eckhardt[22]. Having been obtained a traveling-wave edge state in a domain of $(L_x, L_z) = (2\pi, 2\pi)$ at $Re = 1400$, we adopt an initial condition 16 periodically connected (see Figure 4.1.) As a result of the edge tracking, a streamwise localized edge state has been observed as shown in Figure 4.3. It can be considered that the trajectory has converged by using the initial condition close to the stable manifold of the edge state. A long wave instability can lead to the different state from the traveling wave edge state in a short streamwise computational domain (see Melnikov *et al.* 2014[48] and Chantry *et al.* 2014[49]). As shown in the trajectory of

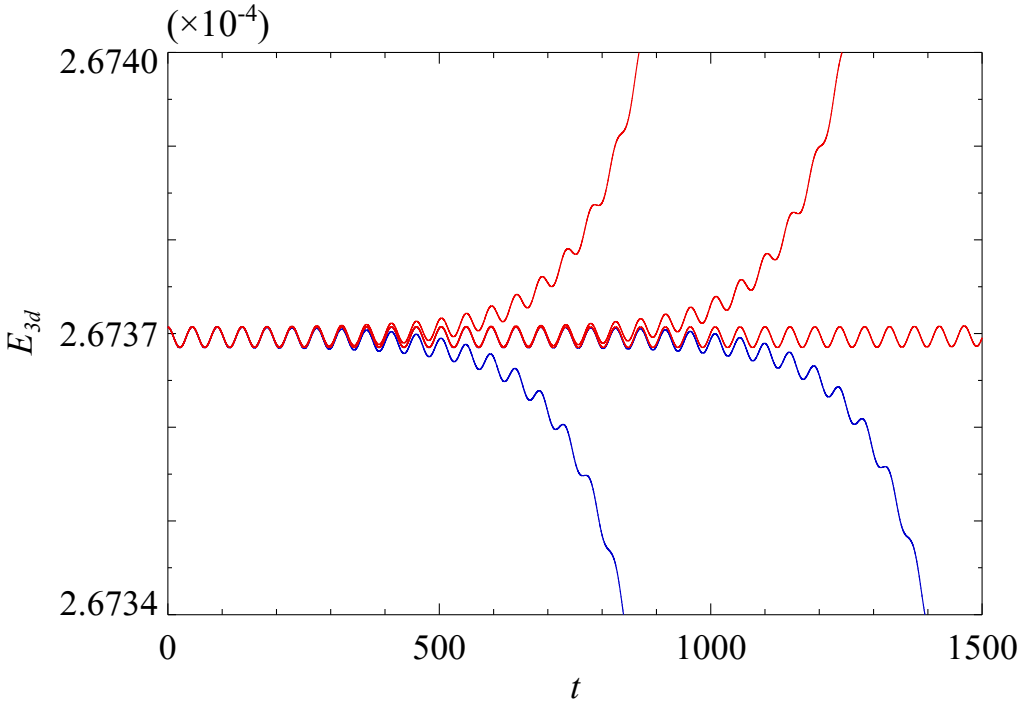

Figure 4.2: Energy trajectories near the edge state in the domain of $(L_x, L_z) = (32\pi, 2\pi)$ at $Re = 1400$. These trajectories turn turbulent (red) and laminar (blue), respectively.

the energy E_{3d} in Figure 4.2, we observed that the periodic solution fluctuates with very small amplitude of $\mathcal{O}(10^{-9})$. Using the Newton-Krylov hookstep method, we confirm the period $T \simeq 91.74$, that is, two periods in Figure 4.2. Figure 4.3-(b) shows the streamwise velocity distribution on mid-plane and the near wall $y \simeq 0.6$ and the streamwise vorticity on $y \simeq 0.2$. The spatial structure has the streamwise vortices in the leading edge region and the low-speed streak in the trailing edge region. The reason for two period fluctuation in Figure 4.2 can be explained that the wavy structure of the leading edge forms the reflection symmetric arrangement in terms of the spanwise direction after one period. Paying attention to the spatial structure of streamwise vortices, Figure 4.4-(a) which shows the streamwise verocity distribution with vector field on y-z cross section at (A)-(C) indicates the strong spanwise velocity near the mid-plane region. That is, the streamwise vortices can be arranged by the shear in the spanwise direction. The streamwise-averaged cross-section in Figure 4.4-(b) shows that the streamwise localized edge state has a mirror symmetry in the wall-normal direction. While the traveling wave solution in a smaller domain which we have employed has a shift-reflection symmetry in the streamwise direction, this localized solution does not adopt.

Based on the above characteristic, the streamwise localized edge state is consistent with the result which Zammert & Eckhardt[22] have reported. They have tracked this solution expanding the computational domain in the spanwise direction but they have reported that it is not an edge state due to the appearance of a new unstable mode. However, as shown in following statement, we have indicated

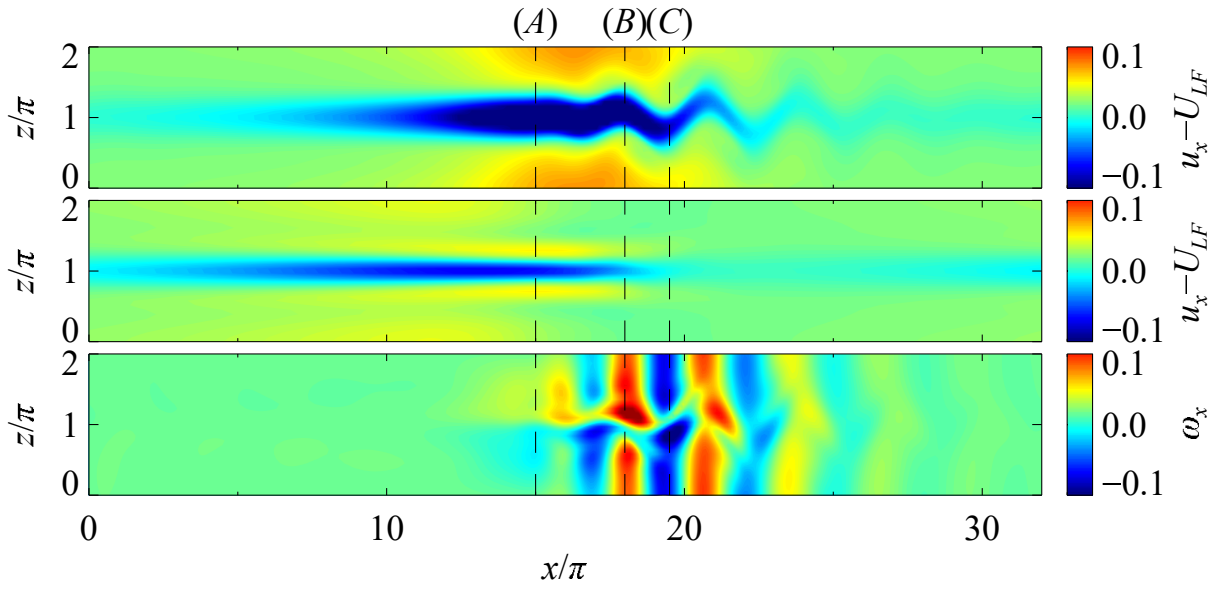

Figure 4.3: Distribution of streamwise velocity (top and center) and streamwise vorticity (bottom) in the edge state of the domain $(L_x, L_z) = (32\pi, 2\pi)$ at $Re = 1400$: (top) mid-plane; (center) $y \simeq 0.6$; (bottom) $y \simeq 0.2$.

that a doubly localized edge state.

In order to discuss the growing and development process of localized turbulence, the existence of streamwise and spanwise localized solution is indispensable. For searching it, we employ the Newton-Krylov hookstep iteration. However, in this tracking method, since we are not able to judge whether the solution is an edge state, we carry out the linear stability analysis and investigate the number of unstable modes. In our study, we employ the Arnoldi iteration[25] to compute eigenmodes.

We start from a relative periodic solution in a computational domain of (L_x, L_z)= $(32\pi, 4\pi)$ in which the maximum wavenumbers are taken as (J, K, M)=$(170, 47, 31)$ for the tracking. Following the smaller spanwise domain, we search a traveling wave edge state in $(L_x, L_z) = (2\pi, 4\pi)$ at $Re = 2000$ and periodically connect it to be an initial condition in the longer domain. Using the edge tracking and the Newton-Krylov hookstep to identify the period, a periodic edge state of $T \simeq 101.00$ have been observed as shown in Figure 4.5. The spatial structure does not have noticeable difference from that of the edge state in $(L_x, L_z) = (32\pi, 2\pi)$ but there is a sign of localization in the spanwise direction.

Then starting with it as an initial state, we track the solution by the Newton-Krylov hookstep iteration expanding the spanwise numerical domain. Figure 4.6 shows the invariant solution localized in the streamwise and spanwise directions in a domain of $(L_x, L_z) = (32\pi, 6\pi)$ in which the maximum wavenumbers are taken as $(J, K, M) = (170, 47, 47)$ at $Re = 2000$ visualized by the streamwise velocity distribution on the mid-plane and the near wall region $y \simeq 0.7$. We consider the

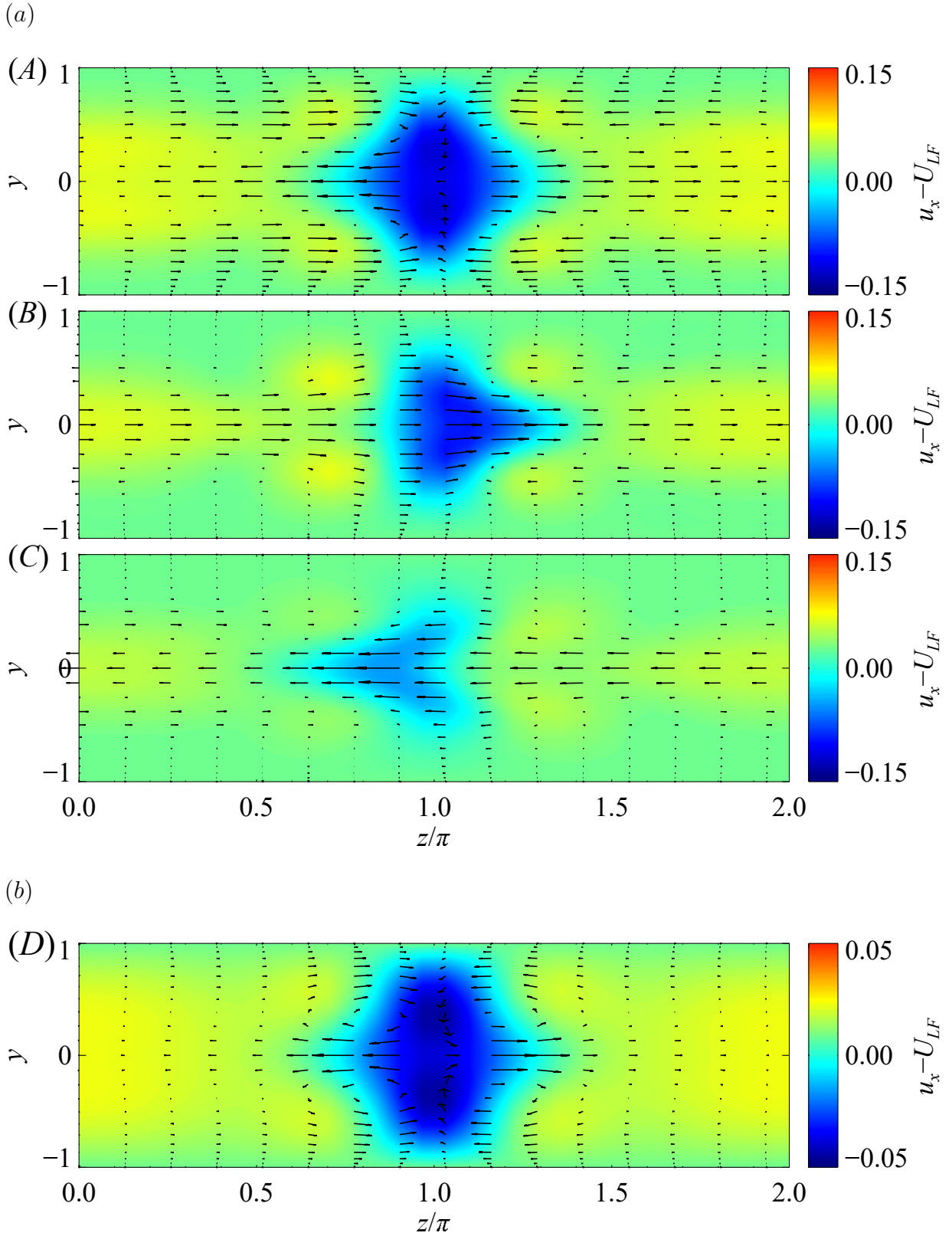

Figure 4.4: (a): Cross-sections in the edge state of the domain of $(L_x, L_z) = (32\pi, 2\pi)$ at $Re = 1400$ at the streamwise position indicated in Figure4.3 (A)-(C). (b) Streamwise-average.

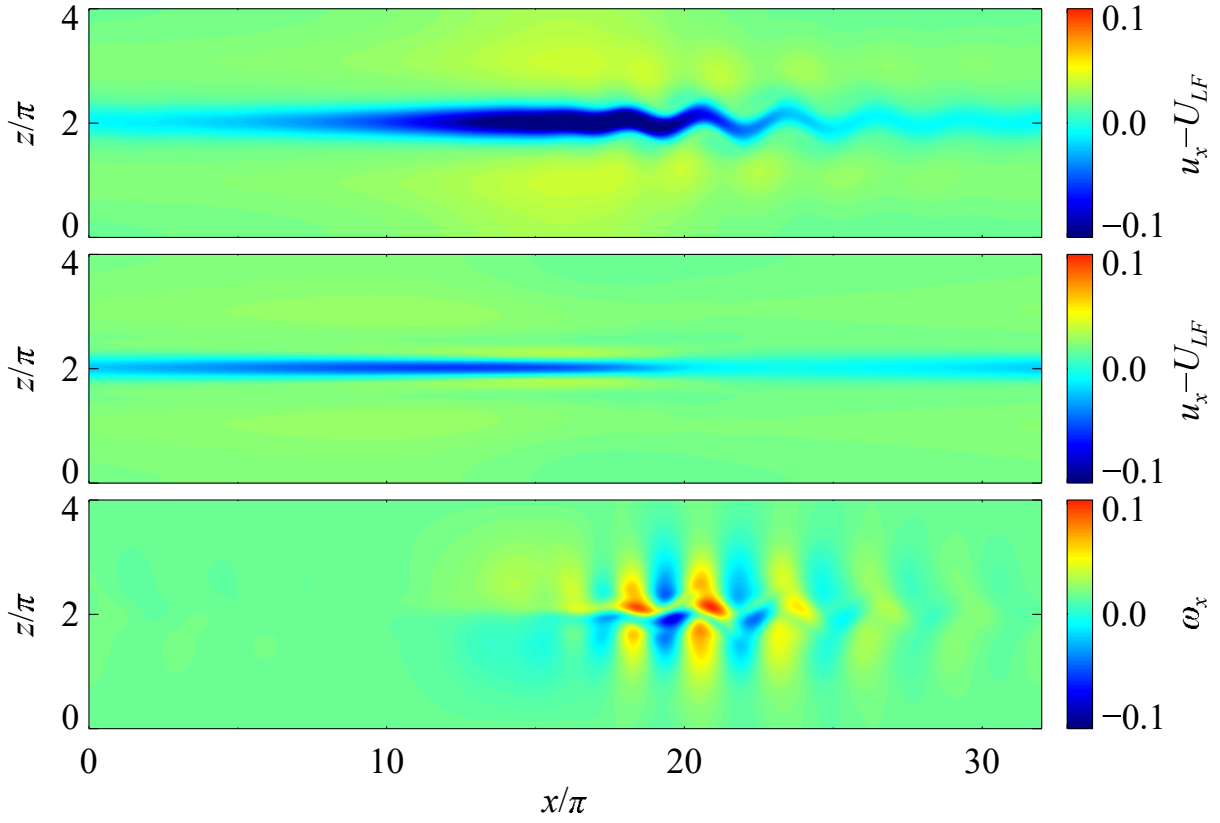

Figure 4.5: Distribution of streamwise velocity (top and center) and streamwise vorticity (bottom) in the edge state of the domain of $(L_x, L_z) = (32\pi, 4\pi)$ at $Re = 2000$: (top) mid-plane; (center) $y \simeq 0.6$; (bottom) $y \simeq 0.2$.

energy density $E_{sp}(z)$ defined as

$$E_{sp}(z) = \frac{1}{4L_x} \int_0^{L_x} \int_{-1}^{1} \left\{ (u_x - U_{LF})^2 + u_y^2 + u_z^2 \right\} dxdy \tag{4.1}$$

and investigate the localization in the spanwise direction as shown in Figure 4.7. Wider the spanwise numerical domain, closer E_{sp} to the laminar state $E_{sp} = 0$ on the boundary condition.

The doubly-localized solution we have obtained can be consistent with Zammert and Eckhardt (2014)[22], however as following, the linear stability analysis indicates a crucial difference from their report. Figure 4.8 shows plots of $\lambda = \exp(\lambda^* T)$ where λ^* is an eigenvalue and T is a period of solution. The unstable mode and stable modes nearest to the unit circle (solid line) of the solution at each L_z are shown in Figure 4.8-(a). Points inside the unit circle are stable modes and outside is unstable. Note that neutral modes about spatial and time shifts are plotted on the circle $(\mathrm{Re}(\lambda), \mathrm{Im}(\lambda)) = (1, 0)$. Figure 4.8-$(b)$ which shows the enlarged view of the nearest to the circle indicates that the eigenvalue considered likely to become unstable remains stable mode. As shown in Figure 4.9, the modulus of the eigenvalue shown in Figure 4.8-(b) does not exceed 1.0. Taking into account this result, we argue that if we extend the computational domain in the

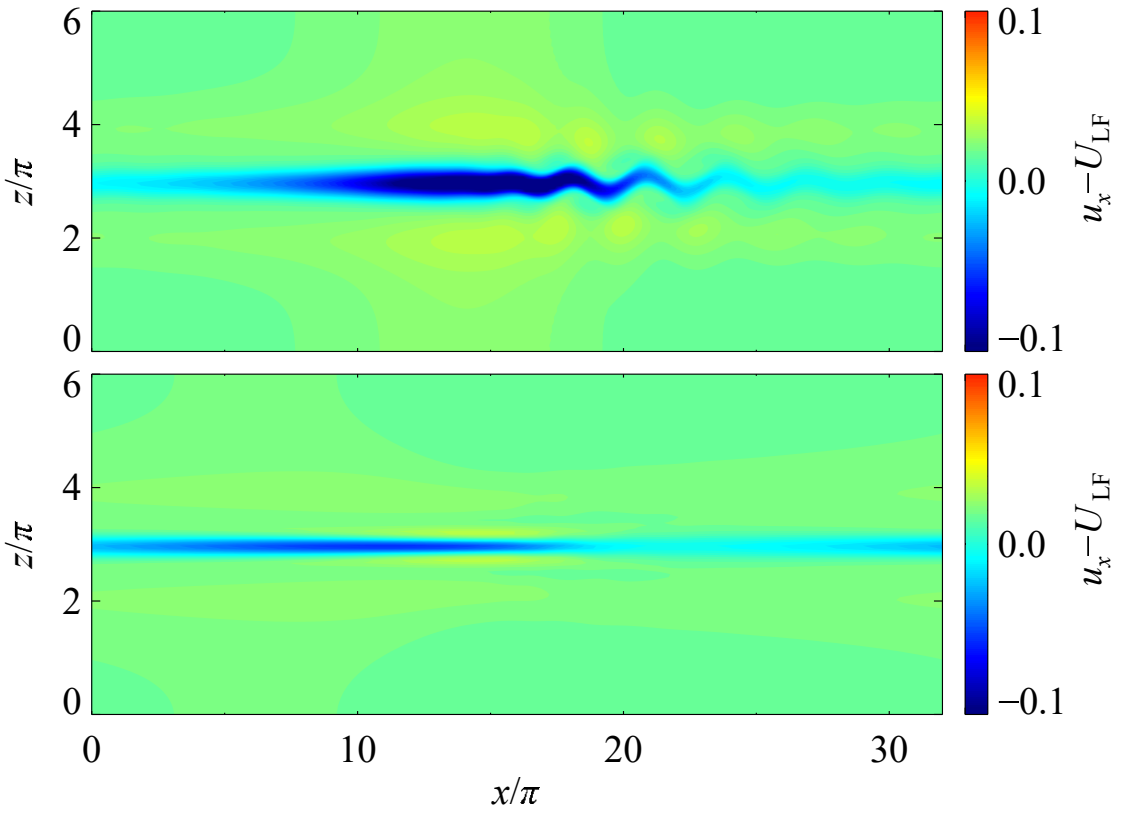

Figure 4.6: Distribution of streamwise velocity (top and bottom) in the edge state of the domain $(L_x, L_z) = (32\pi, 6\pi)$ at $Re = 2000$: (top) mid-plane; (center) $y \simeq 0.7$.

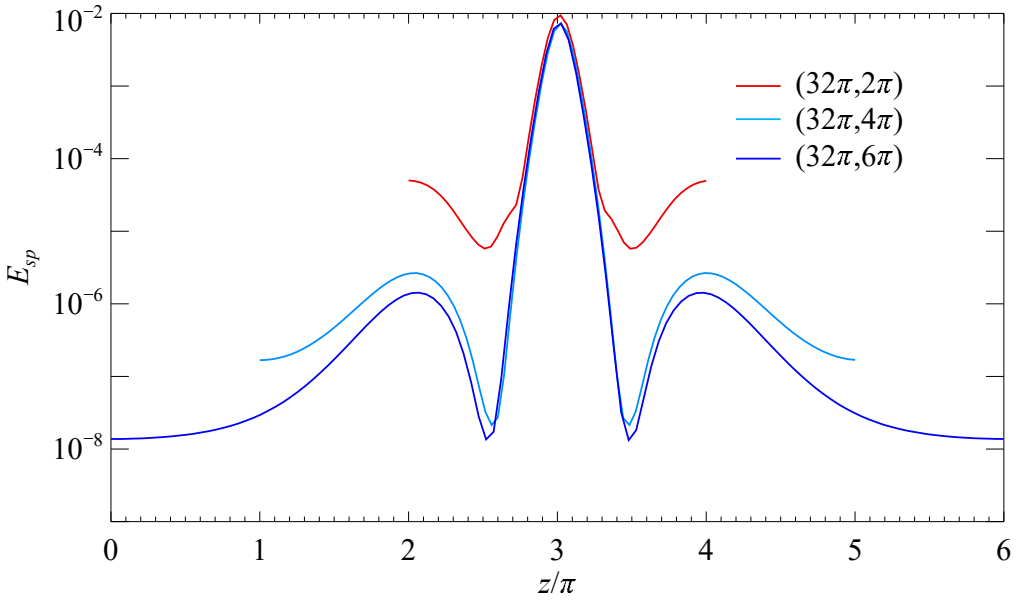

Figure 4.7: Spanwise distribution of total energy of the edge states for various spanwise width L_z and constant streamwise length $L_x = 32\pi$ for $Re = 2000$.

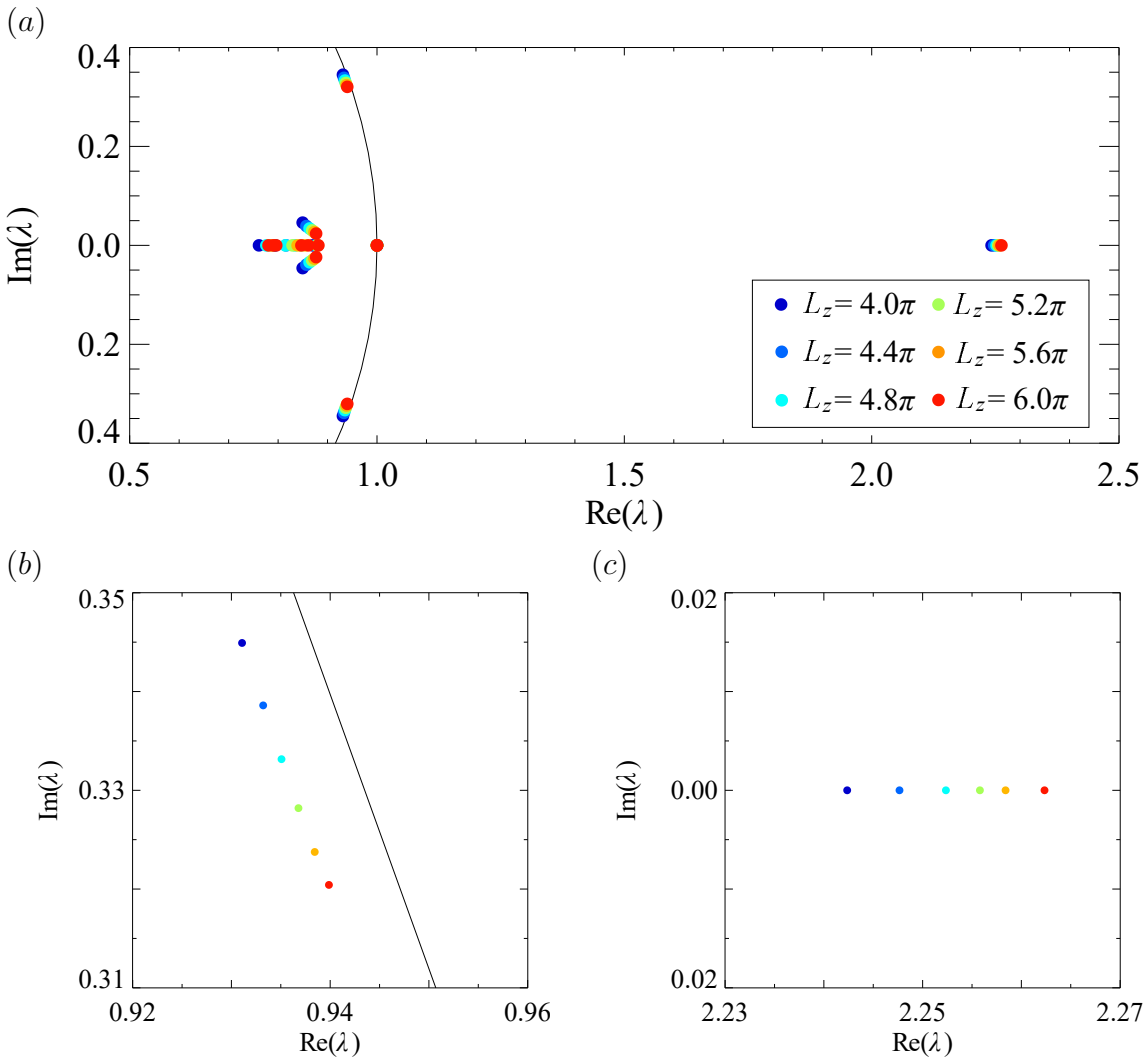

Figure 4.8: (a):Plot of the eigenvalues for various spanwise width L_z. (b)-(c) Magnification of the stable eigenvalue (left) close to the unit circle and unstable eigenvalue (right).

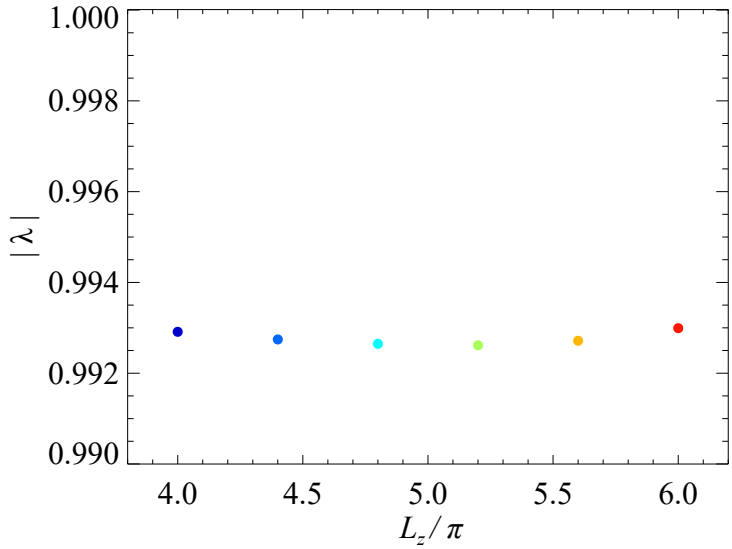

Figure 4.9: The modulus of the stable eigenvalue close to the unit circle.

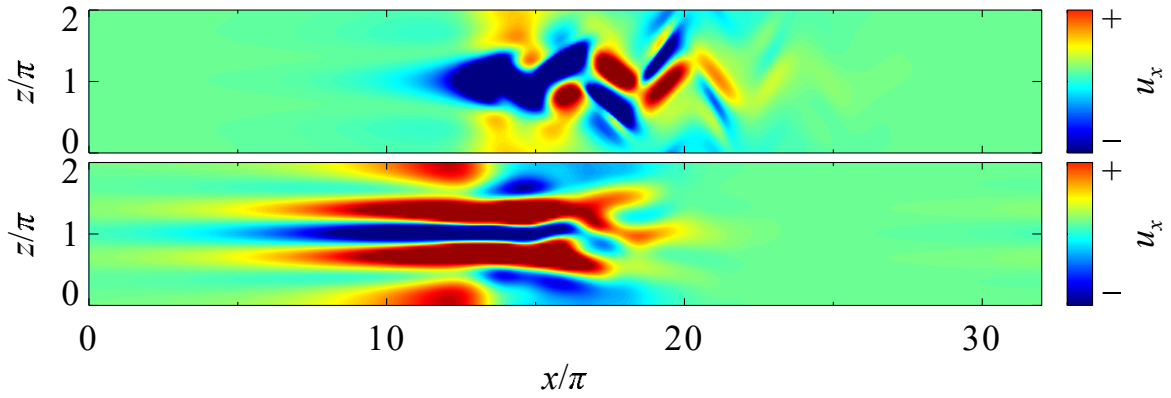

Figure 4.10: Unstable eigenfunction on mid-plane(top) and $y \simeq 0.6$(bottom) in the domain of $(L_x, L_z) = (32\pi, 2\pi)$ at $Re = 1300$.

spanwise direction a spatially localized solution remains an edge state. Zammert and Eckhardt (2014)[22] have reported that the streamwise localized edge state at $Re = 2180$ becomes unstable for $L_z \geq 6\pi$. They also mention that this solution increases its instability at lower Reynolds number. Therefore, we consider the high resolution case and investigate an edge state in $(L_x, L_z) = (32\pi, 6\pi)$ at $Re = 2000$. We set the maximum wavenumber as $(J, K, M) = (255, 47, 63)$ and carry out the Newton-Krylov hookstep and stability analysis. Then the number of unstable mode remains one and we conclude that our solution is a spatially localized edge state.

4.3 Growing process to turbulence

In this section, we investigate how the flow develops from the spatially localized edge state which we have obtained to turbulence and reveal a growing process of a perturbation beyond a critical amplitude. As we consider in §2.2, an edge state can be an important clue to describe a subcritical transition. An edge state and its stable manifold can form a basin boundary between the laminar and turbulent attractor and correspond with a critical amplitude. If a disturbance is introduced beyond the critical amplitude, i.e. above the basin boundary, the state gets closer to an edge state along its stable manifold, that is, any initial condition leads to uniform attraction to an invariant state. After approaching, it shows the decay or development along the unstable manifold. Therefore, the transition process can be explained as transient attraction and subsequent departure from an edge state. In particular, we focus on an unstable manifold and carry on a theoretically describing of the growing to turbulence.

An eigenfunction distribution of the unstable mode gives us an important information about the initial process of transition to turbulence. First, we investigate an unstable eigenmode of an edge state in $(L_x, L_z) = (32\pi, 2\pi)$ at $Re = 1300$, Figure 4.10 represents an eigenfunction about the streamwise velocity on mid-plane and a near-wall region $y \simeq 0.7$. It does not only enhance the spatial structure but also exhibits the appearance of new low-speed streaks in the near-wall region. This

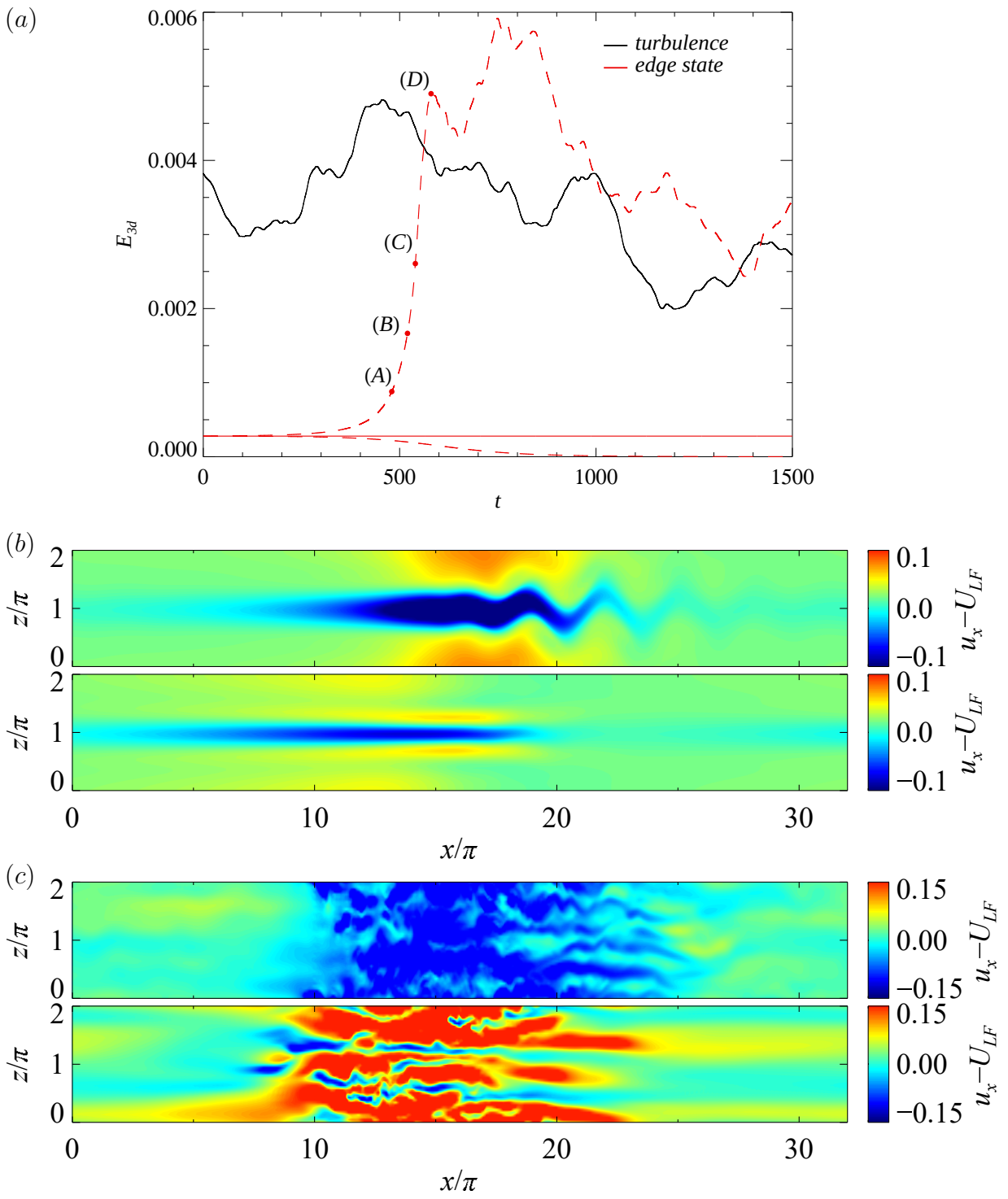

Figure 4.11: (a) Energy trajectories of the turbulence(black) and the edge state(red) in the domain of $(L_x, L_z) = (32\pi, 2\pi)$ at $Re = 1300$. (b)-(c) Snapshots of the turbulence at $t = 500$ indicated in Figure 4.11-(a) and the edge state : (top) mid-plane; (bottom) $y \simeq 0.6$.

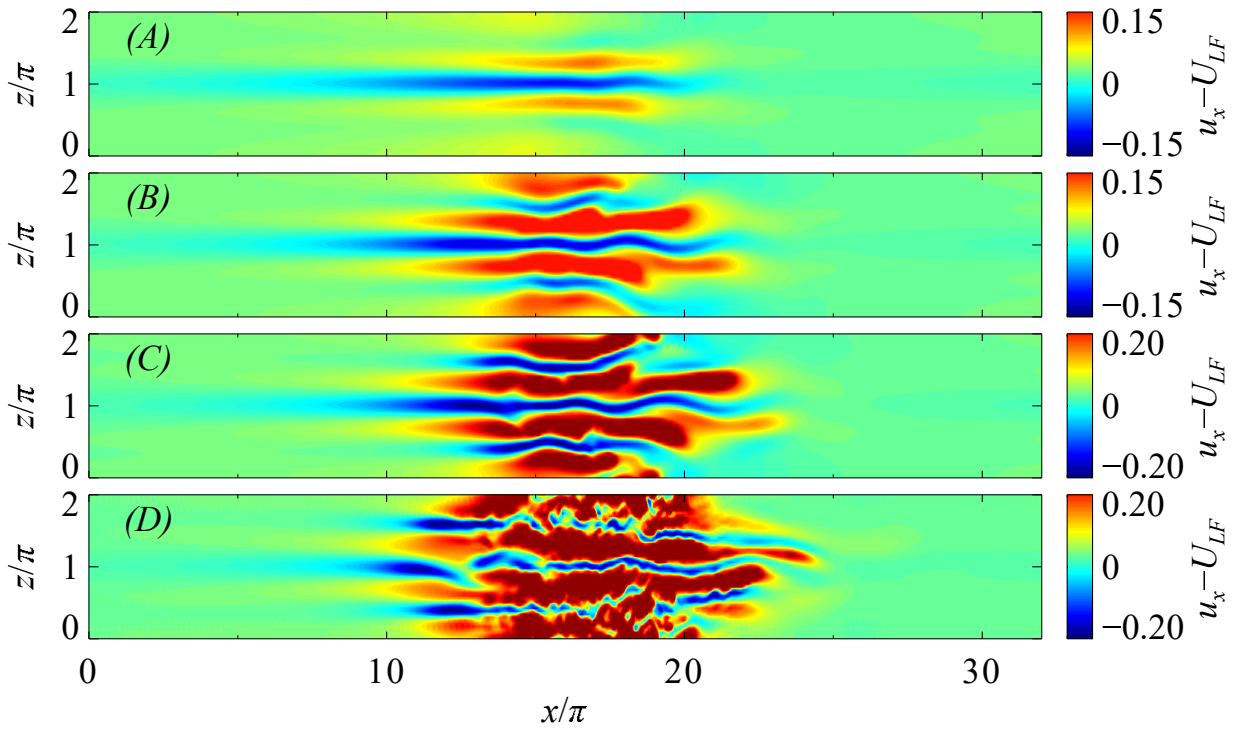

Figure 4.12: Distribution of streamwise velocity flucutuation on near-wall($y \simeq 0.6$) at the point indicated in Figure 4.11-(a).

observation indicates that a disturbance beyond the critical amplitude develops in the spanwise direction. This narrow spanwise computational domain has an influence on spatial periodicity but it can be sufficiently wide to accommodate new low-speed streaks. Therefore, the initial process of the development of localized turbulence is considered to be the appearance of a new coherent structure in the spanwise direction.

Next, we observe the spatial structures developing from the edge state to turbulence and investigate the growing process along the unstable manifold of the edge state. Figure 4.11-(a) shows energy trajectories of turbulence (black) and the edge state (red) at $Re = 1300$ and dotted lines show decay and development from the edge state in which initial conditions are adopted by the edge state added the small unstable eigenmode. Snapshots of turbulence and the edge state are shown in Figure 4.11-(b), (c). Turbulence generated at $Re = 1300$ in this computational domain exists as a turbulent puff localized in the streamwise direction, but at the same time, splitting of puff is also observed. However, we consider that single puff state is regarded as a turbulent state in this region. We expect that the growing process of a flow having a coherent structure such as an edge state into a turbulent state suggests some sort of property in that we can visually grasp a feature. Therefore, we display snapshots growing from the edge state to turbulence. Figure 4.12 shows the spatial structures on the near-wall $y \simeq 0.7$ at points (A)-(D) in Figure 4.11-(a). A sustaining mechanism of localized turbulence can be explained by the shear instability between the low-speed streak and its surrounding fluid (Shimizu and Kida 2009[6]). Paying attention to low-speed streaks in the process from (A)

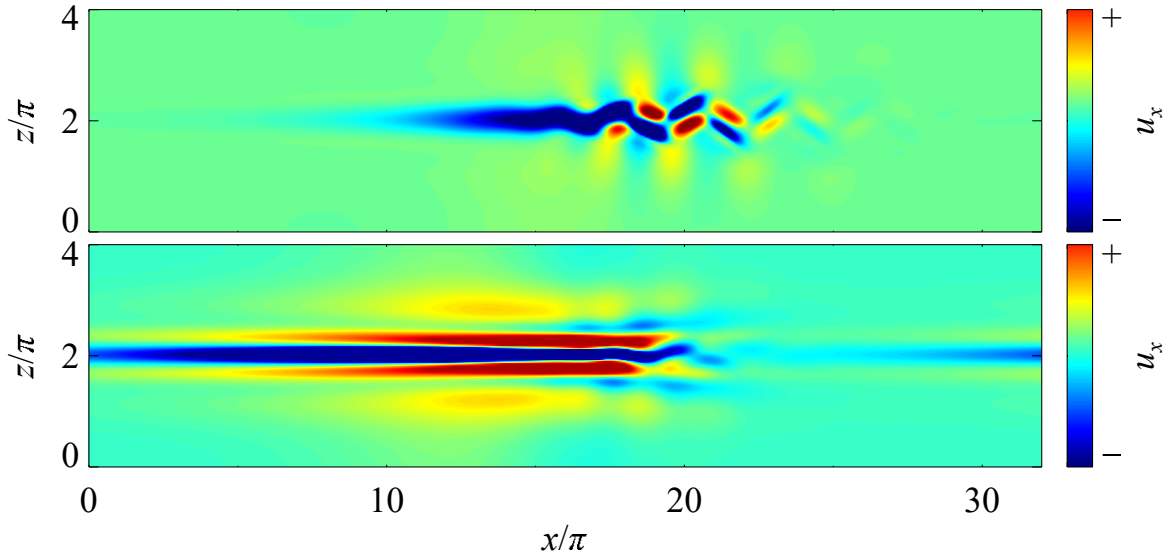

Figure 4.13: Unstable eigenfunction on mid-plane(top) and $y \simeq 0.6$(bottom) in the domain of $(L_x, L_z) = (32\pi, 4\pi)$ at $Re = 2000$.

to (D), a non-linear growing after the initial process described by unstable eigenmode can also be determined as the appearance and development of streaks in the spanwise direction.

Investigating the growing process of a two-dimensionally localized edge state, we describe the path from a localized disturbance to a turbulent spot. Figure 4.13 and Figure 4.14 show the unstable eigenfunction distribution about the streamwise velocity in the region of $(L_x, L_z) = (32\pi, 4\pi)$ and $(L_x, L_z) = (32\pi, 6\pi)$, respectively. As we have discussed above, the enhancement of spatial structures and the appearance of new low-speed streaks can be observed. Spatiotemporal structures under growing on the near-wall are visualized at each domain in Figure 4.15 and Figure 4.16. Shown in these figures, the initial stage of development of turbulence can still be explained as the spanwise growing, but we observe the inclined growing in the streamwise direction. This is the initial stage of V-shaped developments of turbulent spots observed by the experiment (Alavyoon *et al.* 1986[45]) and numerical simulation (Henningson and Kim 1991[46]). Therefore, the non-linear development on the unstable manifold theoretically represents the growing process of the turbulent spot as an actual phenomenon.

4.4 Control of turbulence by adjoint mode

So far, we have investigated the response to an infinitesimal disturbance and subsequent nonlinear growth of the spatially localized edge state. Here, in order to examine the forcing input to realize this development shown in unstable eigenmode, we perform the adjoint eigenfunction analysis. The adjoint eigenfunction represents the most efficient disturbance input to realize the eigenmode which we have investigated (here we call the direct mode). Distributions of direct and adjoint eigenfunction might not be the same in location in the flow. In the previous study,

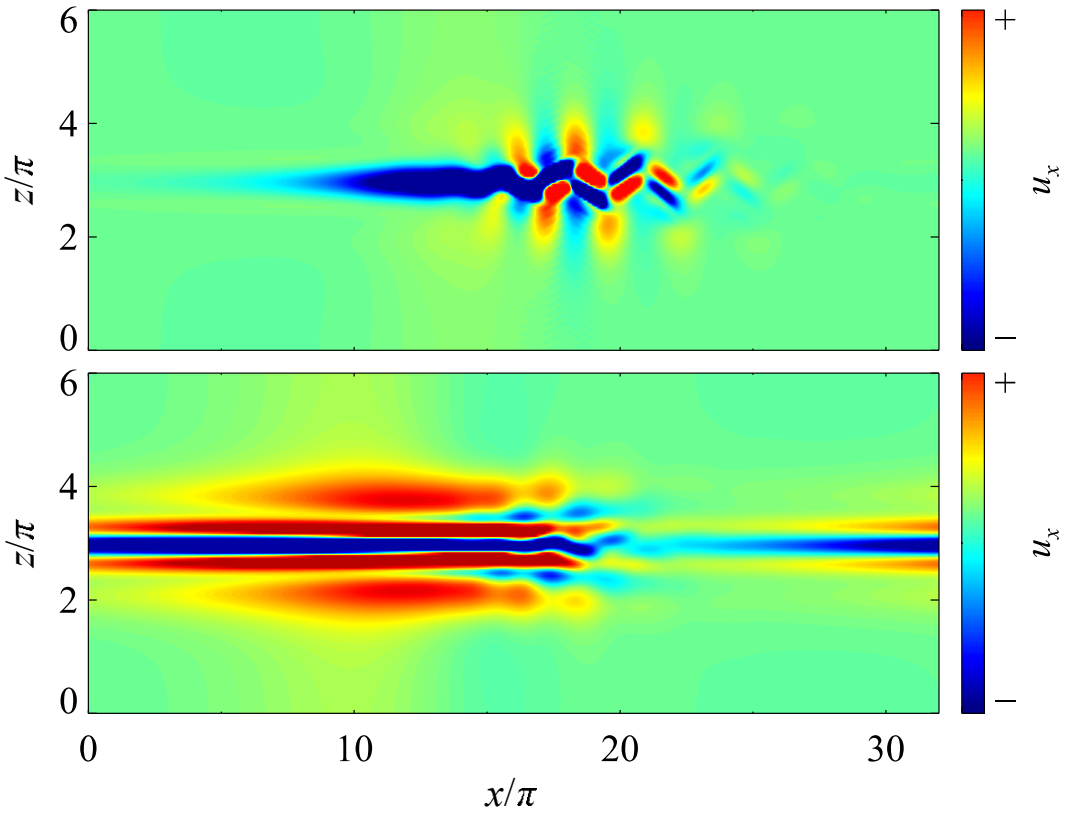

Figure 4.14: Unstable eigenfunction on mid-plane(top) and $y \simeq 0.7$(bottom) in the domain of $(L_x, L_z) = (32\pi, 6\pi)$ at for $Re = 2000$.

a discussion of the cylinder wake instability based on the structural sensitivity of the unstable eigenmode has been provided by Giannetti and Luchini (2007)[50]. It can be very important information where to put the forcing because it is an effective way in order not only to excite but also to decay the flow. Therefore we can expect to obtain the knowledge of control of turbulence.

We solve the adjoint eigenvalue problem by the adjoint Navier-Stokes equations. Deviation processes and numerical methods are described in the Appendix. We carry out the direct and adjoint eigenvalue analysis of the spatially localized edge state in the domain of$(L_x, L_z) = (32\pi, 6\pi)$ discussed in §4.2. Figure 4.17 shows the spatial distribution of the edge state, the direct eigenfunction and the adjoint eigenfunction, respectively. The direct mode is visualized by the streamwise velocity distribution and the adjoint mode is the wall-normal velocity distribution. Focusing on the adjoint eigenfunction, the forcing enhancing low-speed streaks appears in the near-wall region. In the direct mode, that spatial distribution can be shown in the streamwise velocity, that is, it seems that the influence of the input in the wall-normal direction appears as a decrease of the streamwise velocity and the low-speed streaks are enhanced. Therefore, we can simply explain that the input enhancing edge state has an effect on the low-speed streaks which is a core of sustaining mechanism of turbulence. In the experiment, input in the wall-normal direction corresponds to injection, for example jet on the wall, so it seems that it is a simple way as a control of turbulence. In the center region of the wall, the

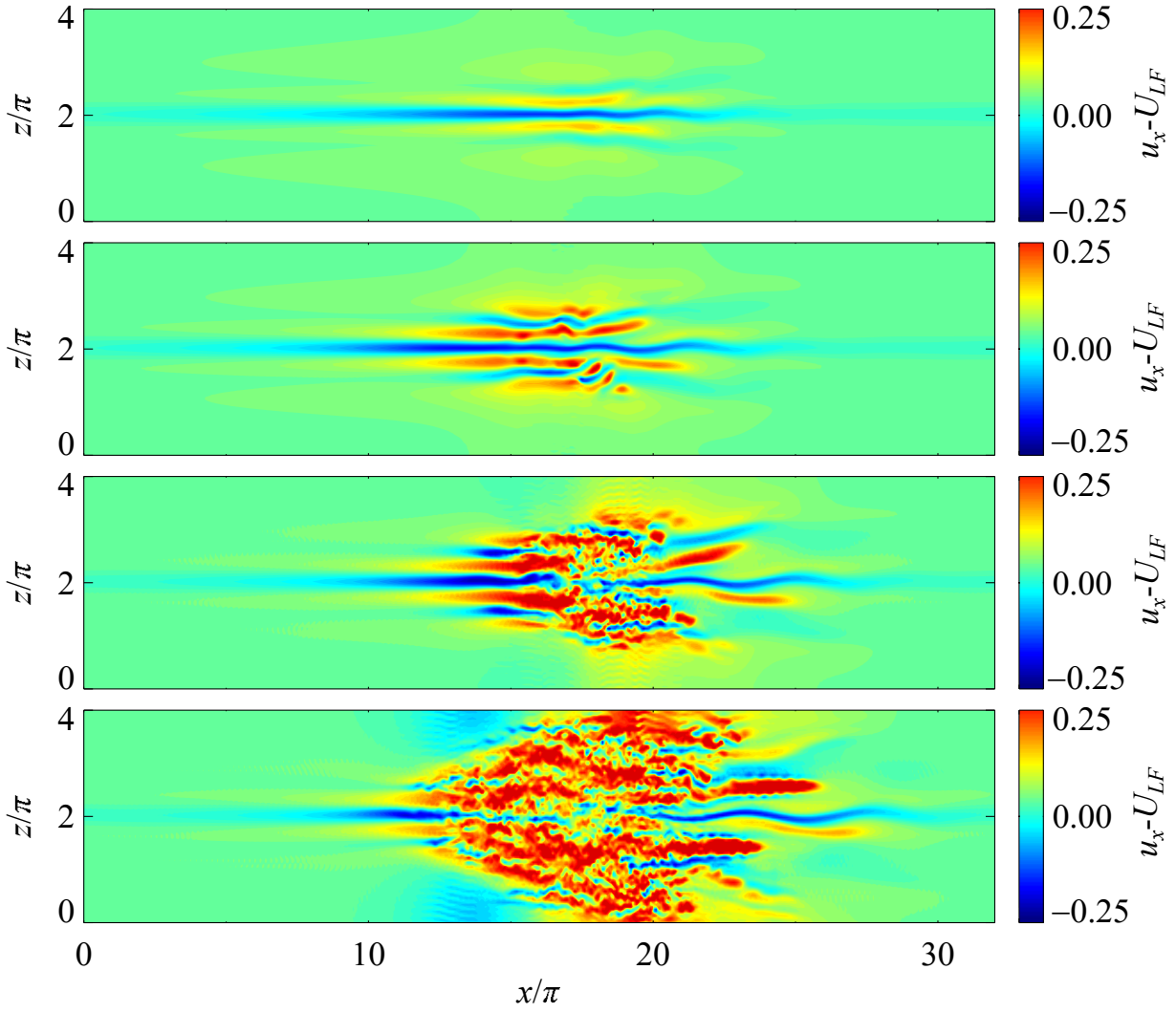

Figure 4.15: Temporal evolution of flow structure turning into turbulence indicating streamwise velocity fluctuation on $y \simeq 0.6$ in the domain of $(L_x, L_z) = (32\pi, 4\pi)$ at for $Re = 2000$.

forcing is distributed upstream of the edge state and direct mode because of the mean advection in plane channel flow. However, in real control, it is impractical to apply an external force near the center region.

4.5 Conclusion

In this chapter, we carry out the direct numerical simulation of plane channel flow and attempt to describe the subcritical transition to turbulence. Since properties of an edge state which is an invariant solution having one unstable mode can be a clue to explain that difficult problem, we investigate this solution and carry out the stability analysis. As an interpretation of an edge state, there is also an attempt to identify the onset of turbulence by tracking the solution with respect to the Reynolds number and identifying the bifurcation structure (Kreilos

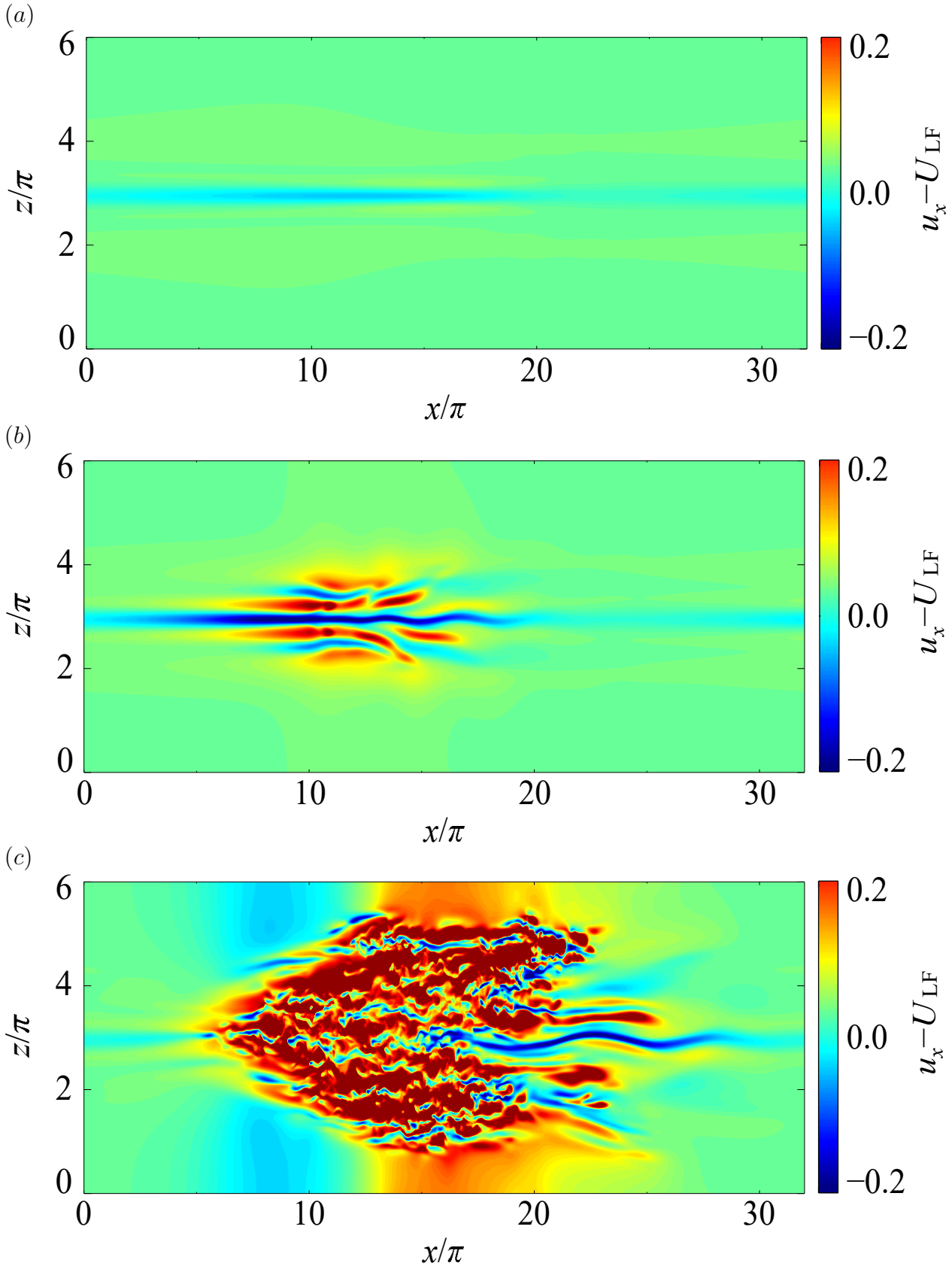

Figure 4.16: Temporal evolution of flow structure turning into turbulence indicating streamwise velocity fluctuation on $y \simeq 0.7$ in the domain of $(L_x, L_z) = (32\pi, 6\pi)$ at $Re = 2000$.

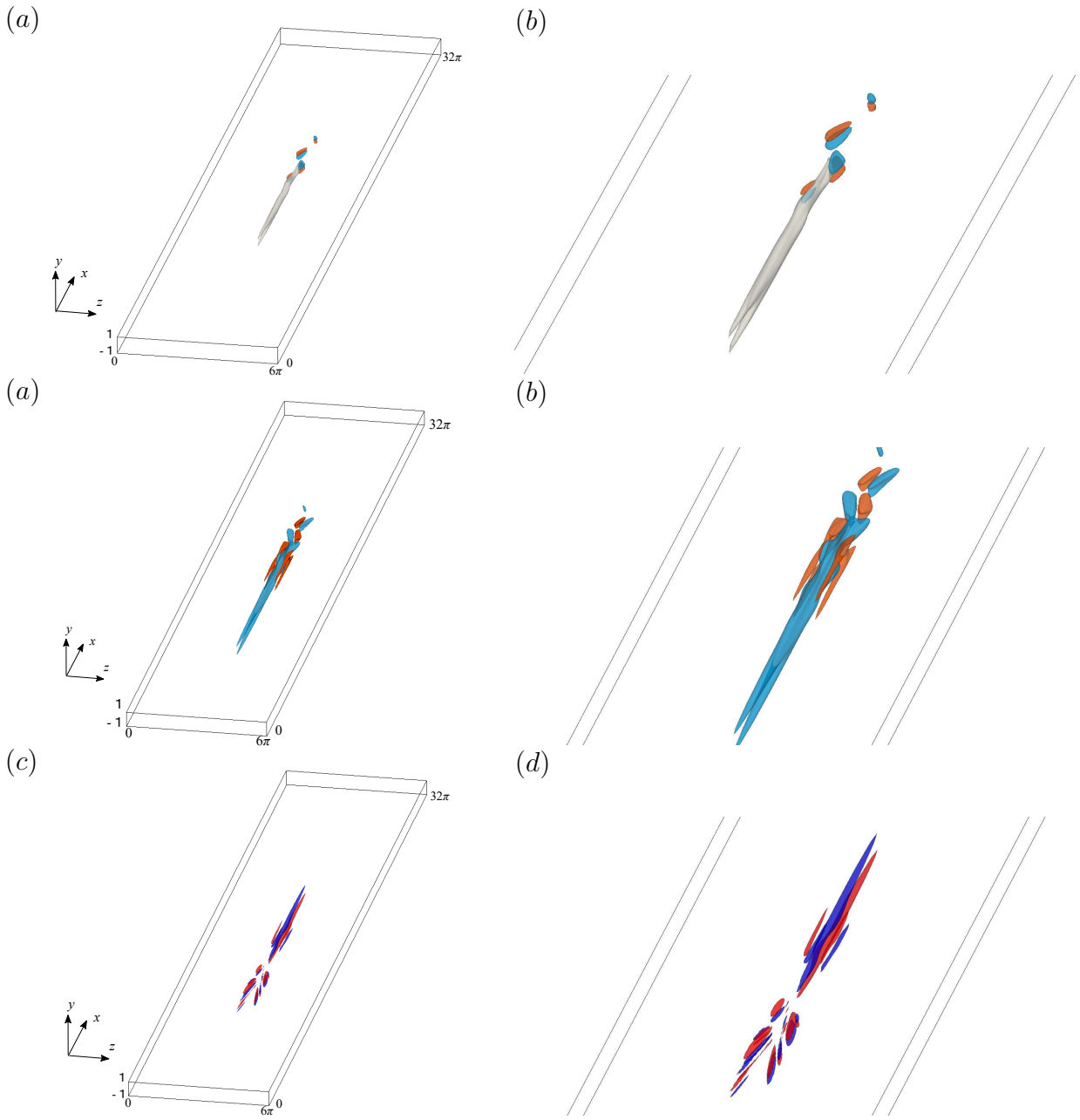

Figure 4.17: Spatial structures in the edge state, direct eigenmode and adjoint eigenmode in the domain of $(L_x, L_z) = (32\pi, 6\pi)$ for $Re = 2000$. (a)-(b): The edge state. Low-speed streaks are visualized by isosurfaces of streamwise velocity fluctuation (gray), $u_x - U_{LF} = -0.1$. Streamwise votices are visualized by orange (positive) and cyan (negative) isosurfaces, $\omega_x = \pm 0.5 \times 10^{-2}$. (c)-(d): The direct eigenmode. Streamwise velocity distributions are visualized at the value of $u'_x = 3$ (cyan) and $u'_x = -5$ (orange). (e)-(f): The adjoint eigenmode. Wall-normal velocity distributions are visualized at the value of $u_y^+ = \pm 3$ (positive, red: negative, blue.)

and Eckhardt 2012[17], Avila *et al.* 2013[20]). If the edge state is equivalent to the unstable lower branch solution, we can discuss this problem. However the upper branch in our system is a more unstable solution and it can be appropriate. In order to investigate the transition process as an actual phenomenon, we focus on the spatially localized edge state.

We observe the spatially localized edge state in the streamwise and spanwise directions by tracking the solution extending the spanwise direction from the streamwise-localized edge state (Zammert and Eckhardt 2014[22]). The stability analysis indicates that the spanwise extension of numerical domain does not contribute to the increase of unstable mode. We examine the higher resolution case but the spatially localized solution remains the edge state.

Next, we examine the unstable mode of the edge state and observe the initial process in which a disturbance beyond the critical amplitude grows. It can be explained by the appearance of low-speed streaks and spanwise expanding. This scenario does not depend on disturbances because of properties of an edge state. As an additional discussion, we consider the adjoint eigenmode and investigate where to input forcing in the best way. The input in the wall-normal direction on the wall is important for the growth of the disturbance of the edge state, that can be a guide for the control of turbulence.

While we describe a transition process from a localized disturbance to a turbulent spot, by further growing, a turbulent band has been observed (Tsukahara *et al.* 2005[8]; Tsukahara *et al.* 2014[51]; Tuckerman *et al.* 2014[47].) The process how band structure is formed is indispensable issue about transition to turbulence in plane channel flow. In next chapter, we investigate a growing and sustaining mechanism of a turbulent band.

Chapter 5

Sustaining and growing mechanism of localized turbulent band in plane channel flow

5.1 Introduction

In wall-bounded shear flow, transition to turbulence triggered by finite-amplitude perturbations has been studied for over a century with no fundamental breakthrough since full nonlinearity of subcritical transition complicates our understanding, unlike supercritical case. A typical description of subcritical transition is given by a formulation of localized turbulence surrounded by a laminar state and a development of a turbulent region. In pipe flow, a streamwise localized turbulence called turbulent puff exhibits a splitting (Avila *et al.* 2011[3]), a slug development (Duguet *et al.* 2010[5]) and decay depending on the Reynolds number. It can be regarded as one dimensional development. Recent studies have shown that it exhibits the one dimensional dynamical model like the $(1+1)$D directed percolation (DP) model (Barkley 2011[52]; Sipos and Goldenfeld 2011[53]) or the predator-prey model (Shih *et al.* 2016[54]). In plane channel flow or plane Couette flow, on the other hand, a two-dimensionally localized turbulent spot can grow in the streamwise and spanwise directions, that is, more complex two dimensional development. As is the case with the pipe flow, it is suggested that transition process to turbulence is related to the universal class of directed percolation (Lemoult *et al.* 2016[55]; Sano and Tamai 2016[56]).

The purpose of this study is to reveal the growing and sustaining mechanism of localized turbulence in plane channel flow. An initial perturbation larger than the threshold distinguishing between growth and decay follows some development stages. Unless the low Reynolds number a turbulent spot shows a monotonic growth to a turbulent band (Tsukahara *et al.* 2005[8]) inclined in the streamwise direction. In the process of this development the two dimensionally localized turbulent bands can appear (Xiong *et al.* 2015[41]). The demonstration of generation and sustaining mechanisms of such localized turbulence is an important clue for understanding the transition process in channel flow.

In this chapter, we investigate numerically the sustaining mechanism of turbulent bands. In §5.2, we discuss the behavior of localized turbulent band in a large computational domain. Based on the result of former section, we focus on the downstream edge of the band and analyze it in §5.3. Concluding remarks and discussions are presented in §5.4.

5.2 Sustaining turbulent band in large numerical domain

The development of localized turbulence at lower Reynolds numbers is explained by the growth of turbulence in an oblique direction (Xiong *et al.* 2015[41]). If the numerical domain is moderate and the aspect ratio defined by the ratio of the length to the width is a certain value (Tsukahara *et al.* 2005[8]), the growing turbulence eventually catches up with itself and can be connected periodically to form a turbulent band. However, in order to investigate the growing process of turbulence as an actual phenomenon, a large numerical domain is required so as to prevent a band from being influenced by the surrounding flow field including its own. In our study, the numerical domain is set in each direction to $(L_x, L_z) = (500, 250)$ for which the maximum wavenumbers are taken as $(J, K, M) = (1279, 47, 639)$, so that periodically connected bands are not formed even for a long integration time. Moreover, another important problem is concerned with the lower critical Reynolds number at which sustaining turbulence is observed. It has been suggested by the equilibrium of the time scale of the decay and the splitting (Avila *et al.* 2011[3]) or the rise of the turbulent fraction (Sano and Tamai 2016[56]; Lemoult *et al.* 2016[55]). However, in our study, we carry out a long time calculation for one initial condition and define it as which turbulence does not decay.

We consider the localized turbulence like the 'seed' [41] as an initial condition. It corresponds to turbulence at the early stage at which a turbulent spot develops to a turbulent band. When the Reynolds number is slightly higher, the turbulent spot can show the V-shaped development (Aida *et al.* 2011[57]) but in this study we consider the lower Reynolds number, so that all the initial conditions grow in one direction and less interaction with the flow field can be expected. As a result of calculation at various Reynolds numbers and observation the state of turbulence, we have found sustaining turbulence at $Re_m \gtrsim 440$. This value is lower than the estimated critical value (Carlson *et al.* 1982[7]; Sano and Tamai 2016[56]) and that this turbulence seems to include an important coherence in the transition problem. Interestingly, the sustaining turbulence we observe is a localized turbulent band. Therefore, we investigate the time variation of the length of the band. The streamwise length ℓ_x and the spanwise length ℓ_z of the band structure are obtained from the distribution of the average of kinetic energy in the streamwise direction $u'^2_{\{x,z\}}(\{z,x\}) = \frac{1}{L_{\{z,x\}}} \int_0^{L_{\{z,x\}}} (u_x(x,0,z) - U_{LF})^2 \, d\{z,x\}$. A region larger than a certain threshold is defined as a band and the length is determined. Figure 5.1-(a) shows the streamwise length ℓ_x and the spanwise length ℓ_z of the localized turbulent and the angle $\theta = \tan^{-1}(\ell_z/\ell_x)$ with respect to the

(*a*)

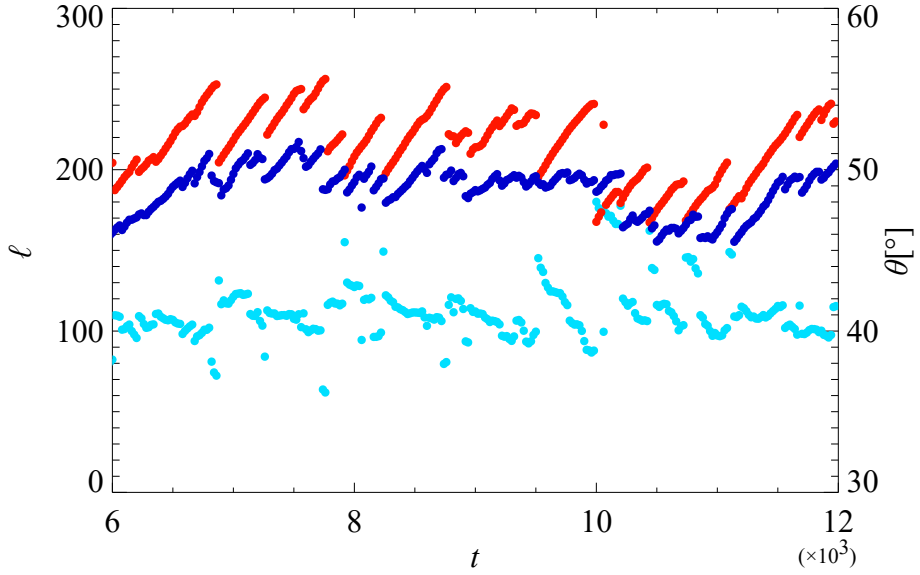

(*b*)

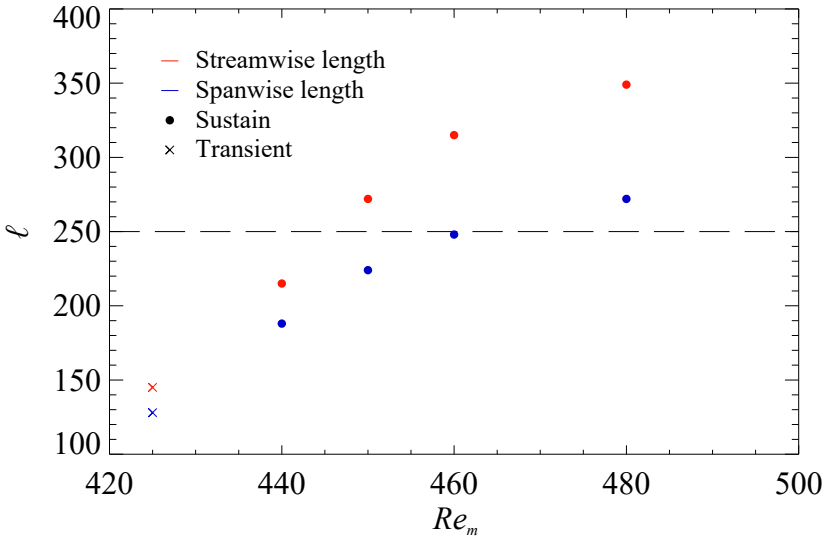

Figure 5.1: (a) The length of an isolated turbulent band in the streamwise (ℓ_x, red) and spanwise (ℓ_z, blue) direction and the angle of the band ($\theta = \tan^{-1}(\ell_z/\ell_x)$, cyan) as a function of time. (b) The time averaged length in the streamwise and spanwise direction as a function of Re_m. The dashed line denotes the spanwise numerical domain L_z.

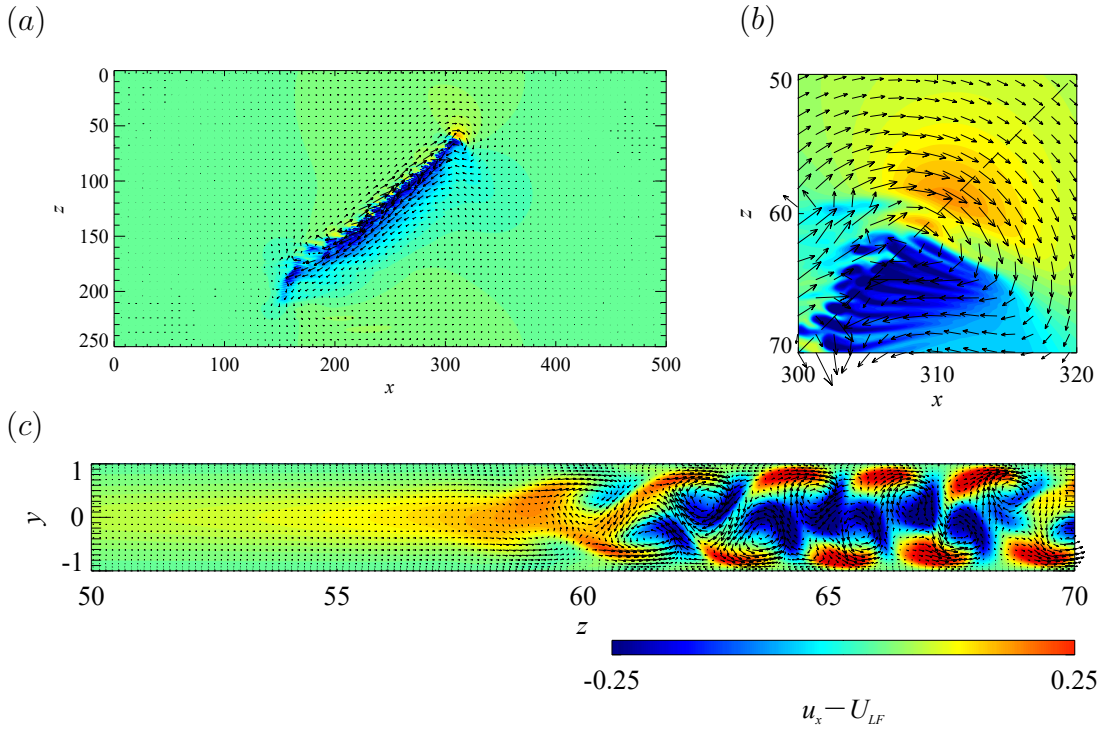

Figure 5.2: (a) The snapshot of an isolated turbulent band at $Re_m = 440$ shown by the streamwise-velocity fluctuation with arrows indicating the large-scale flow. (b) The downstream end of an isolated turbulent band. (c) The distribution of streamwise velocity fluctuation near the downstream edge shown by arrows indicating the projection of the cross-streamwise velocity of (y, z) plane on dotted line plane shown in Figure 5.2-(b). This figure is reprojected (y, z) plane.

streamwise direction. It takes the value of 40°∼45° and the time average angle in this figure is approximately 41°. This value is a constant value before growing band becomes an equilibrium state. The periodically connected band is inclined by about 20° to 30° with respect to the streamwise direction (Tsukahara *et al.* 2014[51]), but it can be observed that the angle becomes larger when localized also in the longitudinal direction. The localized turbulence like an equilibrium puff will change the state such as decay and splitting in a certain finite time, but since the turbulence observed in our investigation is maintained for a very long time, it must have different properties. That is, it can be regarded as a kind of attractor. Figure 5.1-(b) shows the Reynolds number dependence of the length of the structure in the spanwise direction and the streamwise direction of the localized band that was statistically in equilibrium. Up to $Re_m = 460$, the average length of the turbulent structure increases linearly with Reynolds number but increases thereafter gently after that. This means that the length of the structure is about L_z, which is the spanwise numerical domain so that there is nearby disturbance (though it is itself) due to periodicity. As a result, it is considered that the increase in the length of the structure became slowly due to the influence of the interaction.

A localized turbulent band has a certain characteristic spatial structure. We

analyze an instantaneous flow field of a localized turbulent band at $Re_m = 440$. Figure 5.2-(a) is the snapshot indicated by the streamwise velocity fluctuation $u_x - U_{LF}$ on $y = 0$ and wall-normal averaged cross-section flow on x-z plane $\mathbf{u}(x, z) = \frac{1}{2}\int_{-1}^{1}(u_x - U_{LF}, u_z)\, dy$. The large-scale flow moves downstream along the band in upper stream side and opposite in downstream side (Duguet and Schlatter 2013[58]). In the localized case, the large-scale flow shows the circulation around a band. As we can see from that, focusing on the downstream edge of the band, there is the high-velocity region faster than the laminar flow. The extended view Figure 5.2-(b) explains that the high velocity patch exists at the end of a turbulent structure seems to be an oblique wave. We can see that this patch generates the turbulent band. Figure5.2-(c) shows the velocity distribution of the cross-section shown by the dashed line in Figure5.2-(b). The streamwise velocity fluctuation $u_x - U_{LF}$ is shown by the color contour and the arrow indicates the projection of the cross-streamwise velocity on the (y, z) plane. The high speed region of the center between the walls propagate in the streamwise and spanwise direction leaving a staggered array of quasi-periodically generating counterrotating tubular vortices which will be left behind to become chaotic, forming a turbulent band. Therefore the downstream edge of the band is involved in the growth mechanism of a turbulent band.

5.3 Periodic motion in downstream edge

The generation of quasi-periodic disturbance from the high speed region in the downstream edge is considered to be the mechanism of generation of turbulence in the localized turbulent band. The band we have observed is formed by obliquely continuing disturbances with the high speed region and the turbulence emitted from it as a building block. In other words, we expect that there exist some coherent structures embedded in the downstream region. Therefore, we consider extracting this building block from the localized turbulent band. As an extraction method, let us consider the following approach. Paying attention to the downstream edge of the band, turbulence is generated from the high speed patch to the upstream region. Therefore, we attempt to carry out the extraction of the downstream edge from localized band by removing the upstream turbulent region by an external forcing. Here we consider the following governing equations with the spatially distributed damping term.

$$\frac{\partial \Delta u_y}{\partial t} = -\left(\nabla \times \left(\nabla \times (\boldsymbol{u} \times \boldsymbol{\omega})\right)\right)_y + \frac{1}{Re}\left(\Delta^2 u_y\right) - \alpha f(x, z, t)\, \Delta u_y \quad (5.1)$$

$$\frac{\partial \omega_y}{\partial t} = \left(\nabla \times (\boldsymbol{u} \times \boldsymbol{\omega})\right)_y - \alpha f(x, z, t)\, \omega_y \quad (5.2)$$

$$\frac{\partial}{\partial t}\frac{\partial^2 \phi_x}{\partial y^2} = \frac{\partial}{\partial y}\left\langle (\boldsymbol{u} \times \boldsymbol{\omega})_x \right\rangle_{xz} + \frac{1}{Re}\frac{\partial^4 \phi_x}{\partial y^4} - \alpha f(x, z, t)\left(\frac{\partial^2 \phi_x}{\partial y^2} - \frac{\partial U_{LF}}{\partial y}\right) \quad (5.3)$$

$$\frac{\partial}{\partial t}\frac{\partial^2 \phi_z}{\partial y^2} = \frac{\partial}{\partial y}\left\langle (\boldsymbol{u} \times \boldsymbol{\omega})_z \right\rangle_{xz} + \frac{1}{Re}\frac{\partial^4 \phi_z}{\partial y^4} - \alpha f(x, z, t)\frac{\partial^2 \phi_z}{\partial y^2}, \quad (5.4)$$

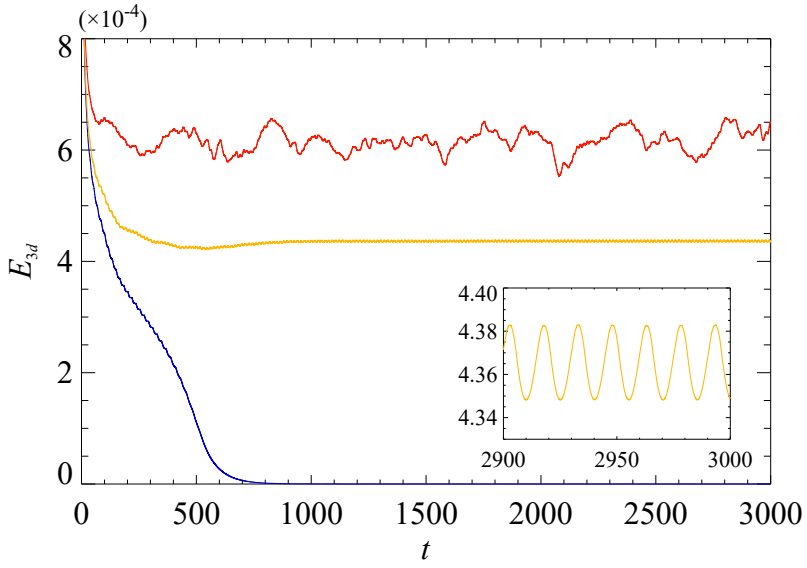

Figure 5.3: Time evolution at $Re_m = 450$ depending on damping parameter d. The red, yellow and blue colored trajectories represent $d \simeq 20.83, d \simeq 18.23$ and $d \simeq 17.71$, respectively.

where α is a damping intensity and $f(x, z, t)$ is a spatial distribution function using tanh here (Brand and Gibson 2014[21]).

$$f(x, z, t) = \frac{1}{2} \tanh\left(\frac{r - \beta}{\gamma} - 1\right) \tag{5.5}$$

$$r = \sqrt{(x - x_{C'}(t))^2 + (z - z_{C'}(t))^2} \tag{5.6}$$

First, paying attention to the high speed region existing at the downstream edge, the maximum point $C(x_C(t), z_C(t))$ of the streamwise velocity u_x at $y = 0$ is determined. In this research, the coordinates are determined by grid points in real space. Next, a point separated by d in the streamwise direction and the span direction along the oblique stripe from C is defined as the center $C'(x_{C'}(t), z_{C'}(t)), x_{C'} = x_C - d, z_{C'} = z_C + d$ of the region to be damped. β and γ are coefficients that determine the range of damping. In the area of $r < \beta - \gamma$, the distribution function becomes $f(x, z, t) \approx 1$, and the effect of damping appears. And in $\beta - \gamma < r < \beta + \gamma$, the influence of the attenuation term is smoothly reduced, and in the sufficiently distant area, the damping effect is ignored. As an initial condition, we choose a short band structure growing from a 'seed'. This prevents the oblique fringe turbulence from being torn out and splitting into two bands due to the effect of damping.

We perform DNS changing the distance d at fixed parameters $\alpha = 0.1$, $\beta = 50$ and $\gamma = 10$ in the domain of $(L_x, L_z) = (100, 100)$ in which the maximum wavenumbers are taken as $(J, K, M) = (1279, 47, 639)$. Figure 5.3 shows the result of calculating at $Re_m = 460$. As shown by the blue orbit in this figure, if d is small and the position of damping is close to the downstream edge, turbulence decay to

be laminarized. At a larger d than a certain value, however, it can be decayed and sustained, that is, by extracting only the downstream region, a sustaining edge can be realized. Therefore, it seems that an important mechanism that sustains a localized turbulent band is inherent in the downstream edge. Furthermore, as shown by the yellow orbit in Figure 5.3, by adjusting to $d \simeq 18.23$, a periodic orbit has been obtained. That expects the coherent structures in the downstream edge of a localized turbulent band enable to detect the onset of turbulence by bifurcation analysis in a minimal turbulence in a small domain (Kreilos and Eckhardt 2012[17]). Since this spatial structure sustains with comparatively simple coherence, sustaining mechanism of a localized turbulent band might be described easier. Figure 5.4-(a) shows the wall-normal velocity $u_y$distribution and the large-scale flow mentioned at Figure 5.2-(a). The extracted turbulence is the oblique wave region at the downstream edge (Carlson *et al.* 1982[7]), and it can be seen that the circulation around the turbulent flow still exists. The distribution of the magnitude of large-scale flow in Figure5.4-(b) shows that turbulence is sufficiently localized in the streamwise and the spanwise directions, and it is considered that it is sufficient for the numerical domain.

We carry out the tracking of the downstream periodic motion changing the values of the parameters. Figure5.5-(a) shows the Reynolds number dependence of solutions at a fixed damping parameter $\alpha = 0.1$. Each point is plotted at the local maximum of kinetic energy E_{3d}. The periodic solution in Figure5.5-(a) is an attractor which corresponds to the upper branch solution and the lower branch solution is the edge state obtained by edge tracking (Itano and Toh 2003[13]; Skufca *et al.* 2006[24]). These solutions originate from a saddle-node bifurcation at $Re_m \simeq 448.01$. Note that this critical value depends on damping parameter and filter coefficients. By increasing the Reynolds number, the upper branch solution becomes a torus orbit at $Re_m \simeq 465$ and eventually chaotic orbits. In our system, there are no crisis phenomena such as an occurrence of transient turbulence (Kreilos and Eckhardt 2012[17]). Figure 5.6 shows snapshots of upper branch and lower branch solutions visualized by same thresholds at $Re_m = 460$ in Figure 5.5-(a). We can see no distinguishing differences except active and gentle spatial structures of each branch.

Next, we attempt to track the solution by decreasing the damping parameter α at fixed Reynolds number $Re_m = 460$. If tracking is possible down to $\alpha = 0$, we can discuss the origin of a fully-localized solution in the pure Navier-Stokes system. Figure 5.5-(b) shows the result of tracking starting from the upper branch at $(Re_m, \alpha) = (460, 0.1)$ in Figure 5.5-(a). Decreasing the parameter a torus solution appears at $\alpha \simeq 0.88$, but it returns to the periodic solution again at $\alpha \simeq 0.50$ and turns at saddle-node point $\alpha = 0.046$. Investigating the relationship with the Navier-Stokes equations, we also consider the dependence of the solution on the distance parameter d. Figure 5.7 shows the tracking result of the upper branch solution at $Re_m = 450$ and $\alpha = 0.1$. A periodic orbit appears at $d \simeq 18.23$ (see also Figure 5.3) by a saddle-node bifurcation. Slightly increasing the distance, $d \simeq 18.49$, a torus orbit is observed and finally a chaotic state is obtained at $d \gtrsim 18.75$. At a further larger distance, turbulence does not decay and continues to develop becoming a localized turbulent band. If the spatial periodicity can be

(a)

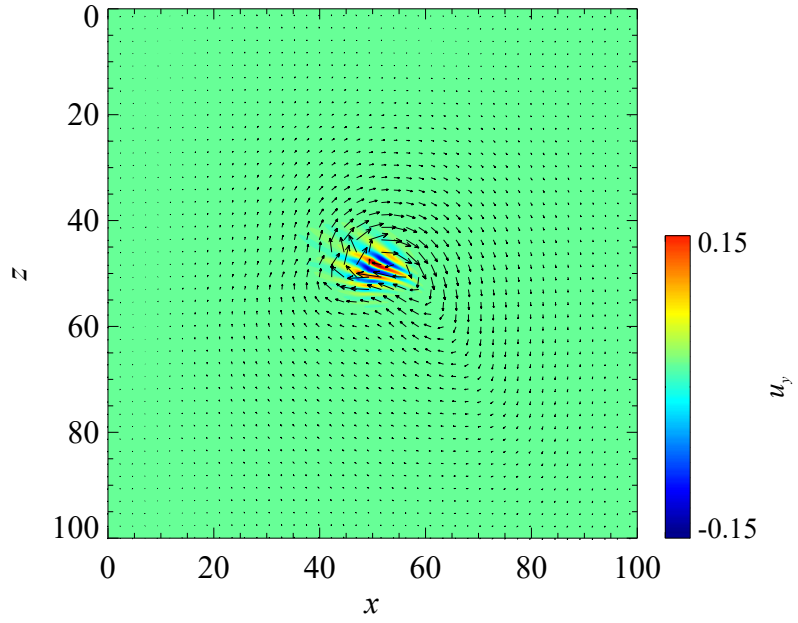

(b)

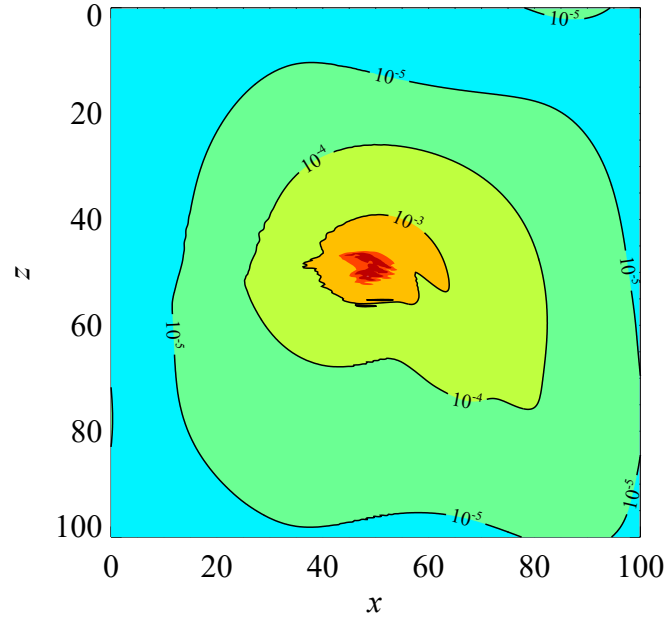

Figure 5.4: Snapshot of a periodic motion shown with yellow colored trajectory in Figure 5.3. (a) Contour plot of wall-normal velocity u_y which varies from -0.15 to 0.15 and vector plot of large scale flow $\bar{\mathbf{u}}\,(x, z)$. (b) Contour plot of magnitude of large scale flow $\bar{\mathbf{u}}\,(x, z)$.

(*a*)

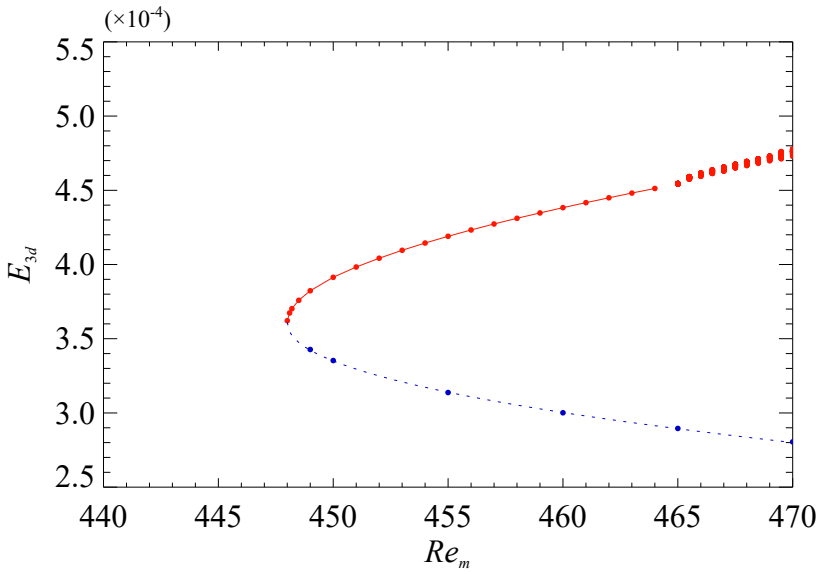

(*b*)

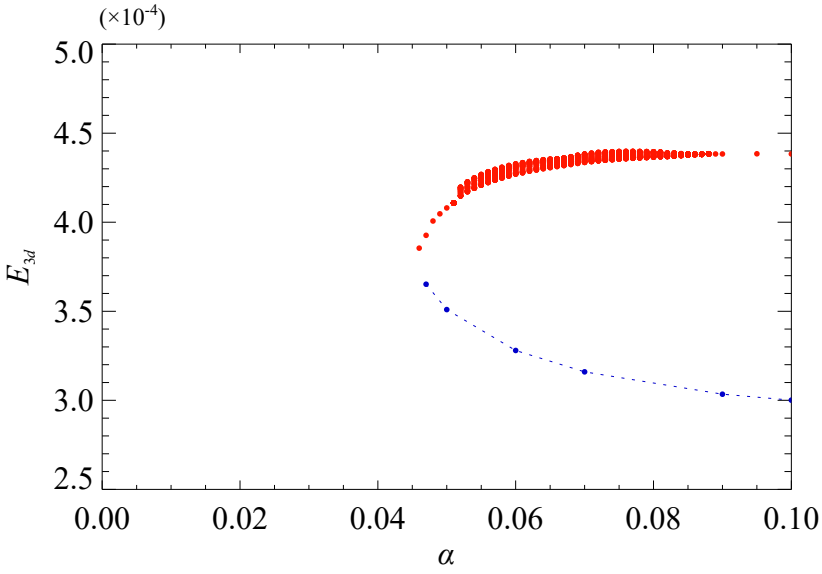

Figure 5.5: Bifurcation diagram. (*a*) E_{3d} as a function of the Reynolds number at fixed dumping coefficient $\alpha = 0.1$. (*b*) E_{3d} as a function the dumping coefficient α at fixed Reynold number $Re_m = 460$.

(*a*)

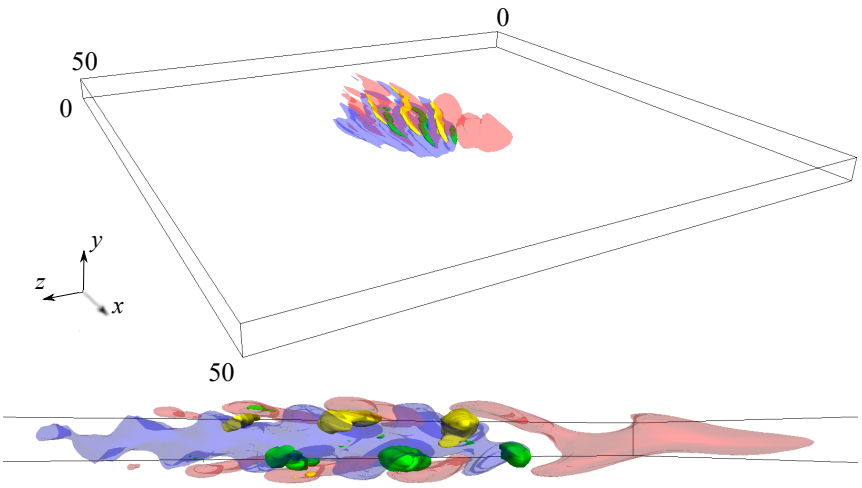

(*b*)

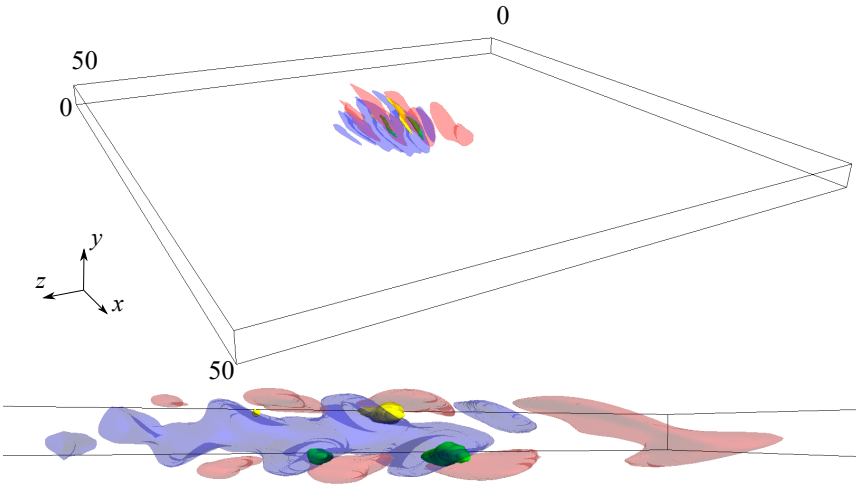

Figure 5.6: Snapshots of the upper branch and lower branch shown in Figure 5.5-(*a*) at $Re_m = 450$. The red and blue isosurfaces represent the streamwise-velocity fluctuation $u'_x = u_x - U_{LF} = \pm 0.1$ (red, $u'_x > 0$; blue, $u'_x < 0$). The yellow and green isosurfaces denote the second invariant of the velocity gradient tensor $q = 0.1$ (yellow, $\omega_x > 0$; green, $\omega_x < 0$).

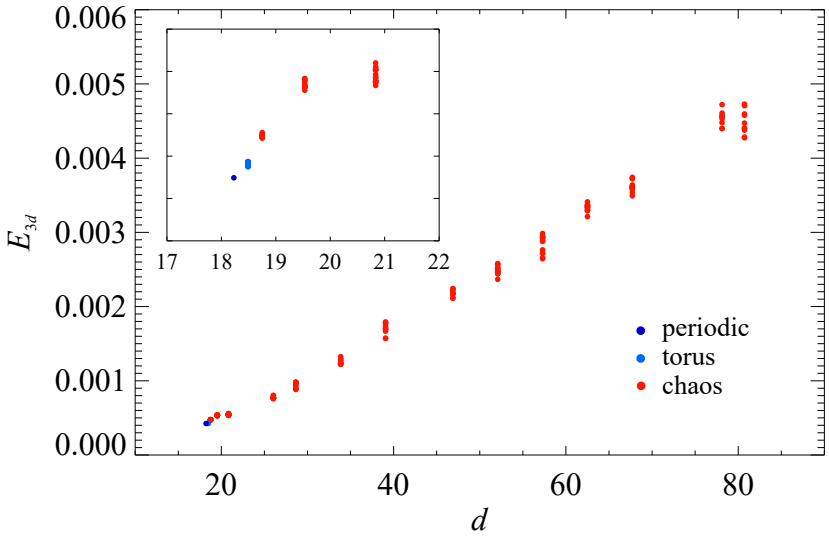

Figure 5.7: E_{3d} as the function of distance d at $\alpha = 0.1$ and $Re_m = 450$. Periodic solutions arise at $d \simeq 18.23$, torus orbits are observed at $d \simeq 18.49$ and chaotic states appear at $d \gtrsim 18.75$.

disregarded, we expect that the turbulent structure extends to the equilibrium length which depends on the Reynolds number (see §5.2). Therefore, we indicate that the turbulent solution arising from the periodic solution could be tracked to the Navier-Stokes system which extinguished the damping term.

5.4 Discussion

In this study, we have performed a large-scale direct numerical simulation of channel flow and observed localized turbulence with oblique structure. There exists a source of disturbances in the downstream edge observed as an oblique wave (Carlson *et al.* 1982[7]) propagating in the streamwise and spanwise directions forming vortex arrays in the upstream region. By balancing the propagating velocity of downstream edge and the decay in the upstream region, localized turbulence has been maintained with a finite length of the structure and a statistical equilibrium state can be realized. This sustaining mechanism is not a cyclic self-sustaining process (Waleffe 1997[59]) but might be characterized by the high-speed region of the downstream edge which constantly continues to generate turbulence. In addition, the Reynolds number where we have observed a sustaining localized band have been lower than the critical value of generating turbulent spots (Carlson *et al.* 1982[7]). Therefore, in the transition problem, it has been important to specify the onset of turbulence. Furthermore, it can be considered that the growing, decay, and equilibrium in a certain direction of turbulence is an exception not applicable to the directed percolation (DP) universality. This can also imply the existence of an equilibrium state at lower Reynolds number than the onset of turbulent fraction (Sano and Tamai 2016[56]).

Removing the upstream turbulent region from a localized turbulent band, periodic dynamics embedded in the downstream end region can be extracted. Since the sustaining mechanism of the downstream edge can be explained by the existence of invariant solutions, this can also be applicable to a localized turbulent band. Applying an artificial external forcing has enabled us to extract coherent structures and thus simplify a complex problem. Therefore, introducing a new parameter, like a rotation number in plane Couette flow, implies that a subcritical transition in Navier-Stokes equations can translate into a supercritical problem.

In the two-dimensional plane channel flow, a stable localized solution has been observed in a long domain (Melibovsky and Meseguer 2015[60]; Teramura and Toh 2016[61]). We analyze the spatial distribution of this two-dimensional solution and confirm that the high speed region exists at the downstream edge. Therefore, we discuss the relationship with the downstream edge region, which plays an important role in the formation maintenance mechanism of the localized turbulent band. Now, we discuss the relationship between a downstream edge solution and a two-dimensional solution. In the two-dimensional case, the vortex in the x-y plane brings about the high speed region, but in the case of three dimensions, it is considered to be based on the circulation of the large flow in the x-z plane. That is, the sustaining mechanism of the high speed region in our study is considered to be unique to three dimensions.

Chapter 6

Conclusion

The purpose of this study is to understand the transition process to turbulence in the wall-bounded shear flow. Identifying the properties of localized turbulence in plane channel flow, we describe the growing process. In this thesis, we approach the three topics. First, we investigate lifetimes of localized turbulence and discuss its relationship with the number of coherent structures. Second work is describing the growing process of a turbulent spot by means of an invariant solution called an edge state. At last, we discuss a localized turbulent band observed after a spot grows and its sustaining mechanism.

6.1 Summary

Exponential growth of lifetime of localized turbulence with its extent in channel flow

In chapter 3, we investigate the dependence of the lifetime on the spanwise extent of the streamwise localized turbulence. For moderate spanwise extent, the lifetime increases exponentially as a function of the aspect ratio. This can be a consequence of near i.i.d (independent and identically distributed) property of turbulent structures. The extreme value theory applied to coherent structures implies that we can determine the threshold to decay. By these result, we might estimate the lifetime of transient turbulence in other systems.

Growing process of localized turbulence in plane channel flow

In chapter 4, we search a spatially localized edge state by using edge tracking algorithm and Newton-Krylov hookstep iteration. Tracking the solution extending the spanwise direction from the streamwise-localized edge state (Zammert and Eckhardt 2014[22]), we have observed a doubly localized edge state. We examine the unstable mode of the edge state and observe the initial process in which a disturbance beyond the critical amplitude grows. The unstable eigenmode shows the appearance of new low-speed streaks leading to growth in the spanwise direction.

This scenario does not depend on disturbances because of properties of an edge state. In addition, we consider the adjoint eigenmode and investigate where to input force in the best way. The input in the wall-normal direction on the wall is important for the growth of the disturbance in the edge state that can be a guide for the control of turbulence.

Sustaining and growing mechanism of localized turbulent band in plane channel flow

In chapter 5, we perform DNS in a large numerical domain and observe a localized turbulent band. A long time integration indicates a sustaining localized band at low Reynolds number $Re_m = 440$. An equilibrium state can be realized by the balance between the propagation of the downstream region in streamwise and spanwise directions and decay of the upstream region. Removing the upstream turbulent region of the band by the spatial damping force, a downstream coherent region exhibiting quasi-periodic behavior in a constantly moving frame of reference is extracted. Its quasi-periodic dynamics consist of the high-speed patch of head region from which vortex arrays are issued. For some appropriate damping parameter, a strictly periodic solution embedded in the downstream region is obtained. This result can describe the sustaining and growing mechanism of a localized turbulent band.

6.2 Future problems

In this thesis, we have investigated behaviors of turbulence in the transitional regime. We can say that a significant part which is the relationship between lifetimes and coherent structures is clarified. Also, we have indicated a forming process from a local disturbance to a turbulent spot and revealed a growing and sustaining mechanism of a localized turbulent band , that is, a core of transition to turbulence in plane channel flow. Such knowledge can be a foothold for control of turbulence.

As we have discussed in chapter 3, lifetimes of streamwise localized turbulence are investigated, however, lifetimes of extended turbulent bands in plane channel flow might not be determined by only coherent structures. A laminar gap of the band can trigger decay to laminar (Manneville 2011[10]), that is, by measuring its emergence and regarding as lifetime we might be able to estimate lifetimes of turbulent bands. Also, an oblique numerical domain (Tuckerman and Barkley 2011[9]) enables us to discuss the band's lifetime.

In chapter 4, we have indicated a doubly localized edge state in plane channel flow. However, the Reynolds number at which it is obtained is higher and we could not track it down to the low Reynolds number. In order to discuss the onset of turbulence, the edge state which can be tracked to low Reynolds number is indispensable. In plane Couette flow (Kreilos and Eckhardt 2012[17]) and pipe flow (Avila *et al.* 2013[20]), it has been reported. In plane channel flow, the localized solution with damping force which we have discussed in chapter 5 might be a

key. We have tracked this solution decreasing the damping coefficient but chaotic bands have been observed. If an invariant solution with no damping force which is a solution to the Navier-Stokes equation can be obtained, it is a breakthrough of transition to turbulence in plane channel flow because it is a doubly localized solution and arises by a saddle-node bifurcation which causes a stable upper branch (attractor) and an unstable lower branch (edge state).

References

[1] O. Reynolds, "An experimental investigation of the circumstances which determine whether the motion of water shall be direct or sinuous and of the law of resistance in parallel channels," *Proc. R. Soc. Lond*, vol. 35, pp. 84–99, 1883.

[2] I. Wygnanski and F. Champagne, "On transition in a pipe. part 1. the origin of puffs and slugs and the flow in a turbulent slug," *Journal of Fluid Mechanics*, vol. 59, no. 2, pp. 281–335, 1973.

[3] K. Avila, D. Moxey, A. de Lozar, M. Avila, D. Barkley, and B. Hof, "The onset of turbulence in pipe flow," *Science*, vol. 333, no. 6039, pp. 192–196, 2011.

[4] M. Shimizu, P. Manneville, Y. Duguet, and G. Kawahara, "Splitting of a turbulent puff in pipe flow," *Fluid Dynamics Research*, vol. 46, no. 6, p. 061403, 2014.

[5] Y. Duguet, A. P. Willis, and R. R. Kerswell, "Slug genesis in cylindrical pipe flow," *Journal of Fluid Mechanics*, vol. 663, pp. 180–208, 2010.

[6] M. Shimizu and S. Kida, "A driving mechanism of a turbulent puff in pipe flow," *Fluid dynamics research*, vol. 41, no. 4, p. 045501, 2009.

[7] D. R. Carlson, S. E. Widnall, and M. F. Peeters, "A flow-visualization study of transition in plane poiseuille flow," *Journal of Fluid Mechanics*, vol. 121, pp. 487–505, 1982.

[8] T. Tsukahara, Y. Seki, H. Kawamura, and D. Tochio, "Dns of turbulent channel flow at very low reynolds numbers," in *TSFP DIGITAL LIBRARY ONLINE*, Begel House Inc., 2005.

[9] L. S. Tuckerman and D. Barkley, "Patterns and dynamics in transitional plane couette flow," *Physics of Fluids*, vol. 23, no. 4, p. 041301, 2011.

[10] P. Manneville, "On the decay of turbulence in plane couette flow," *Fluid Dynamics Research*, vol. 43, no. 6, p. 065501, 2011.

[11] B. Hof, A. de Lozar, D. J. Kuik, and J. Westerweel, "Repeller or attractor? selecting the dynamical model for the onset of turbulence in pipe flow," *Physical review letters*, vol. 101, no. 21, p. 214501, 2008.

[12] M. Avila, A. P. Willis, and B. Hof, "On the transient nature of localized pipe flow turbulence," *Journal of Fluid Mechanics*, vol. 646, pp. 127–136, 2010.

[13] S. Toh and T. Itano, "A periodic-like solution in channel flow," *Journal of Fluid Mechanics*, vol. 481, pp. 67–76, 2003.

[14] F. Waleffe, "Homotopy of exact coherent structures in plane shear flows," *Physics of Fluids*, vol. 15, no. 6, pp. 1517–1534, 2003.

[15] M. Nagata, "Three-dimensional finite-amplitude solutions in plane couette flow: bifurcation from infinity," *Journal of Fluid Mechanics*, vol. 217, pp. 519–527, 1990.

[16] G. Kawahara and S. Kida, "Periodic motion embedded in plane couette turbulence: regeneration cycle and burst," *Journal of Fluid Mechanics*, vol. 449, pp. 291–300, 2001.

[17] T. Kreilos and B. Eckhardt, "Periodic orbits near onset of chaos in plane couette flow," *Chaos: An Interdisciplinary Journal of Nonlinear Science*, vol. 22, no. 4, p. 047505, 2012.

[18] M. Shimizu, G. Kawahara, J. R. Lustro, and L. van Veen, "Route to chaos in minimal plane couette flow," in *Euromech Colloquium EC565 on subcritical transition to turbulence, France*, 2014.

[19] S. Zammert and B. Eckhardt, "Harbingers and latecomers–the order of appearance of exact coherent structures in plane poiseuille flow," *Journal of Turbulence*, vol. 18, no. 2, pp. 103–114, 2017.

[20] M. Avila, F. Mellibovsky, N. Roland, and B. Hof, "Streamwise-localized solutions at the onset of turbulence in pipe flow," *Physical review letters*, vol. 110, no. 22, p. 224502, 2013.

[21] E. Brand and J. F. Gibson, "A doubly localized equilibrium solution of plane couette flow," *Journal of Fluid Mechanics*, vol. 750, 2014.

[22] S. Zammert and B. Eckhardt, "Streamwise and doubly-localised periodic orbits in plane poiseuille flow," *Journal of Fluid Mechanics*, vol. 761, pp. 348–359, 2014.

[23] S. A. Orszag, "Accurate solution of the orr–sommerfeld stability equation," *Journal of Fluid Mechanics*, vol. 50, no. 4, pp. 689–703, 1971.

[24] J. D. Skufca, J. A. Yorke, and B. Eckhardt, "Edge of chaos in a parallel shear flow," *Physical review letters*, vol. 96, no. 17, p. 174101, 2006.

[25] D. Viswanath, "Recurrent motions within plane couette turbulence," *Journal of Fluid Mechanics*, vol. 580, pp. 339–358, 2007.

[26] J. Sánchez, M. Net, B. Garcıa-Archilla, and C. Simó, "Newton–krylov continuation of periodic orbits for navier–stokes flows," *Journal of Computational Physics*, vol. 201, no. 1, pp. 13–33, 2004.

[27] J. E. Dennis Jr and R. B. Schnabel, *Numerical methods for unconstrained optimization and nonlinear equations*. SIAM, 1996.

[28] H. Salwen, F. W. Cotton, and C. E. Grosch, "Linear stability of poiseuille flow in a circular pipe," *Journal of Fluid Mechanics*, vol. 98, no. 2, pp. 273–284, 1980.

[29] V. Romanov, "Stability of plane-parallel couette flow," *Functional analysis and its applications*, vol. 7, no. 2, pp. 137–146, 1973.

[30] A. Schmiegel and B. Eckhardt, "Fractal stability border in plane couette flow," *Physical review letters*, vol. 79, no. 26, p. 5250, 1997.

[31] S. Bottin, F. Daviaud, P. Manneville, and O. Dauchot, "Discontinuous transition to spatiotemporal intermittency in plane couette flow," *EPL (Europhysics Letters)*, vol. 43, no. 2, p. 171, 1998.

[32] H. Faisst and B. Eckhardt, "Sensitive dependence on initial conditions in transition to turbulence in pipe flow," *Journal of Fluid Mechanics*, vol. 504, pp. 343–352, 2004.

[33] B. Hof, J. Westerweel, T. M. Schneider, and B. Eckhardt, "Finite lifetime of turbulence in shear flows," *Nature*, vol. 443, no. 7107, pp. 59–62, 2006.

[34] J. Peixinho and T. Mullin, "Decay of turbulence in pipe flow," *Physical Review Letters*, vol. 96, no. 9, p. 094501, 2006.

[35] A. P. Willis and R. R. Kerswell, "Critical behavior in the relaminarization of localized turbulence in pipe flow," *Physical review letters*, vol. 98, no. 1, p. 014501, 2007.

[36] T. M. Schneider and B. Eckhardt, "Lifetime statistics in transitional pipe flow," *Physical Review E*, vol. 78, no. 4, p. 046310, 2008.

[37] B. Cantwell, D. Coles, and P. Dimotakis, "Structure and entrainment in the plane of symmetry of a turbulent spot," *Journal of Fluid Mechanics*, vol. 87, no. 4, pp. 641–672, 1978.

[38] N. Tillmark and P. H. Alfredsson, "Experiments on transition in plane couette flow," *Journal of Fluid Mechanics*, vol. 235, pp. 89–102, 1992.

[39] A. Prigent, G. Grégoire, H. Chaté, and O. Dauchot, "Long-wavelength modulation of turbulent shear flows," *Physica D: Nonlinear Phenomena*, vol. 174, no. 1, pp. 100–113, 2003.

[40] L. Shi, M. Avila, and B. Hof, "Scale invariance at the onset of turbulence in couette flow," *Physical review letters*, vol. 110, no. 20, p. 204502, 2013.

[41] X. Xiong, J. Tao, S. Chen, and L. Brandt, "Turbulent bands in plane-poiseuille flow at moderate reynolds numbers," *Physics of Fluids*, vol. 27, no. 4, p. 041702, 2015.

[42] J. F. Lawless, *Statistical models and methods for lifetime data*, vol. 362. John Wiley & Sons, 2011.

[43] N. Goldenfeld, N. Guttenberg, and G. Gioia, "Extreme fluctuations and the finite lifetime of the turbulent state," *Physical Review E*, vol. 81, no. 3, p. 035304, 2010.

[44] J. Jiménez and P. Moin, "The minimal flow unit in near-wall turbulence," *Journal of Fluid Mechanics*, vol. 225, pp. 213–240, 1991.

[45] F. Alavyoon, D. S. Henningson, and P. H. Alfredsson, "Turbulent spots in plane poiseuille flow–flow visualization," *The Physics of fluids*, vol. 29, no. 4, pp. 1328–1331, 1986.

[46] D. S. Henningson and J. Kim, "On turbulent spots in plane poiseuille flow," *Journal of fluid mechanics*, vol. 228, pp. 183–205, 1991.

[47] L. S. Tuckerman, T. Kreilos, H. Schrobsdorff, T. M. Schneider, and J. F. Gibson, "Turbulent-laminar patterns in plane poiseuille flow," *Physics of Fluids*, vol. 26, no. 11, p. 114103, 2014.

[48] K. Melnikov, T. Kreilos, and B. Eckhardt, "Long-wavelength instability of coherent structures in plane couette flow," *Physical Review E*, vol. 89, no. 4, p. 043008, 2014.

[49] M. Chantry, A. P. Willis, and R. R. Kerswell, "Genesis of streamwise-localized solutions from globally periodic traveling waves in pipe flow," *Physical review letters*, vol. 112, no. 16, p. 164501, 2014.

[50] F. Giannetti and P. Luchini, "Structural sensitivity of the first instability of the cylinder wake," *Journal of Fluid Mechanics*, vol. 581, pp. 167–197, 2007.

[51] T. Tsukahara, Y. Kawaguchi, and H. Kawamura, "An experimental study on turbulent-stripe structure in transitional channel flow," *arXiv preprint arXiv:1406.1378*, 2014.

[52] D. Barkley, "Simplifying the complexity of pipe flow," *Physical Review E*, vol. 84, no. 1, p. 016309, 2011.

[53] M. Sipos and N. Goldenfeld, "Directed percolation describes lifetime and growth of turbulent puffs and slugs," *Physical Review E*, vol. 84, no. 3, p. 035304, 2011.

[54] H.-Y. Shih, T.-L. Hsieh, and N. Goldenfeld, "Ecological collapse and the emergence of travelling waves at the onset of shear turbulence," *Nature Physics*, vol. 12, no. 3, pp. 245–248, 2016.

[55] G. Lemoult, L. Shi, K. Avila, S. V. Jalikop, M. Avila, and B. Hof, "Directed percolation phase transition to sustained turbulence in couette flow," *Nature Physics*, vol. 12, no. 3, pp. 254–258, 2016.

[56] M. Sano and K. Tamai, "A universal transition to turbulence in channel flow," *Nature Physics*, vol. 12, no. 3, pp. 249–253, 2016.

[57] H. Aida, T. Tsukahara, and Y. Kawaguchi, "Development of a turbulent spot into a stripe pattern in plane poiseuille flow," in *TSFP DIGITAL LIBRARY ONLINE*, Begel House Inc., 2011.

[58] Y. Duguet and P. Schlatter, "Oblique laminar-turbulent interfaces in plane shear flows," *Physical review letters*, vol. 110, no. 3, p. 034502, 2013.

[59] F. Waleffe, "On a self-sustaining process in shear flows," *Physics of Fluids*, vol. 9, no. 4, pp. 883–900, 1997.

[60] F. Mellibovsky and A. Meseguer, "A mechanism for streamwise localisation of nonlinear waves in shear flows," *Journal of Fluid Mechanics*, vol. 779, 2015.

[61] T. Teramura and S. Toh, "Chaotic self-sustaining structure embedded in the turbulent-laminar interface," *Physical Review E*, vol. 93, no. 4, p. 041101, 2016.

Appendix
Adjoint Navier-Stokes equations

In order to construct the adjoint form of incompressible Navier-Stokes equations (NSE), we need to derive the linearized Navier-Stokes equations (LNSE). We decompose the velocity component $\boldsymbol{u}$ and pressure p into a mean part $(\boldsymbol{U}, P)$ and a perturbative part $(\boldsymbol{u}', p')$. Substituted into equations (2.2) and (2.1), LNSE can be expressed as

$$\nabla \cdot \boldsymbol{u}' = 0. \tag{A-1}$$

$$\frac{\partial \boldsymbol{u}'}{\partial t} + \boldsymbol{U} \cdot \nabla \boldsymbol{u}' + \boldsymbol{u}' \cdot \nabla \boldsymbol{U} = -\nabla p' + \frac{1}{Re} \Delta \boldsymbol{u}' \tag{A-2}$$

For distinction from adjoint systems, these equations are referred to as direct LNSE. When performing direct LNSE to solve eigenvalues, $\boldsymbol{U}$ represents a nonlinear solution which we are interested in. Note that, in our study, since our target is a periodic solution it depends on space and time.

Next, we construct the adjoint LNSE. First, we consider the quantities $\boldsymbol{q}'$ and $\boldsymbol{q}^+$ defined as

$$\boldsymbol{q}' = \begin{pmatrix} \boldsymbol{u}' \\ p' \end{pmatrix}, \boldsymbol{q}^+ = \begin{pmatrix} \boldsymbol{u}^+ \\ p^+ \end{pmatrix} \tag{A-3}$$

where $^+$ is the index representing the adjoint system. Therefore, we construct LNSE in terms of $\boldsymbol{q}^+$. In order to simplify equations $(A-2)$ and $(A-1)$ using $\boldsymbol{q}'$, the following operator A is defined as

$$A = \begin{pmatrix} \nabla \cdot & 0 \\ -\dfrac{\partial}{\partial t} - \boldsymbol{NL} + \dfrac{1}{Re}\Delta & -\nabla \end{pmatrix} \tag{A-4}$$

where $\boldsymbol{NL}$ is the operator on nonlinear terms defined as

$$\boldsymbol{NL}\boldsymbol{u}' = (\boldsymbol{U} \cdot \nabla)\, \boldsymbol{u}' + (\boldsymbol{u}' \cdot \nabla)\, \boldsymbol{U} = (\boldsymbol{U} \cdot \nabla)\, \boldsymbol{u}' + (\nabla \boldsymbol{U}) \cdot \boldsymbol{u}'. \tag{A-5}$$

Then equation $(A-2)$ and $(A-1)$ can be rewritten by A and $\boldsymbol{q}'$ following as

$$A\boldsymbol{q}' = \boldsymbol{0}. \tag{A-6}$$

In addition, the spatio-temporal inner product is defined as

$$\left\{\boldsymbol{q}', \boldsymbol{q}^+\right\} \equiv \int_t \int_V \boldsymbol{q}' \cdot \boldsymbol{q}^+ dV dt. \tag{A-7}$$

Conducting the adjoint LNSE from above expressions, as a definition, following relationship is required as

$$\left\{\boldsymbol{q}^{+}, A\boldsymbol{q}'\right\} - \left\{A^{+}\boldsymbol{q}^{+}, \boldsymbol{q}'\right\} = 0 \tag{A-8}$$

where A^{+} represents the operator related to adjoint systems expressed as

$$A^{+} = \begin{pmatrix} \nabla\cdot & 0 \\ \dfrac{\partial}{\partial t} - \boldsymbol{NL}^{+} + \dfrac{1}{Re}\Delta & -\nabla \end{pmatrix}. \tag{A-9}$$

$\boldsymbol{NL}^{+}$ is expressed following as

$$\boldsymbol{NL}^{+}\boldsymbol{u}^{+} = -\left(\boldsymbol{U}\cdot\nabla\right)\boldsymbol{u}^{+} + \left(\nabla\boldsymbol{U}\right)^{T}\cdot\boldsymbol{u}^{+}. \tag{A-10}$$

By substitution, $(A-8)$ can be as

$$\begin{aligned}
&\left\{\boldsymbol{q}^{+}, A\boldsymbol{q}'\right\} - \left\{A^{+}\boldsymbol{q}^{+}, \boldsymbol{q}'\right\} \\
=& \int_t\int_V \boldsymbol{u}^{+}\cdot\left\{-\frac{\partial\boldsymbol{u}'}{\partial t} - \left(\boldsymbol{U}\cdot\nabla\right)\boldsymbol{u}' + \left(\nabla\boldsymbol{U}\right)\cdot\boldsymbol{u}' - \frac{1}{Re}\Delta\boldsymbol{u}' - \nabla p'\right\}dVdt \\
&-\int_t\int_V \left\{-\frac{\partial\boldsymbol{u}^{+}}{\partial t} - \left(\boldsymbol{U}\cdot\nabla\right)\boldsymbol{u}^{+} + \left(\nabla\boldsymbol{U}\right)^{T}\cdot\boldsymbol{u}^{+} - \frac{1}{Re}\Delta\boldsymbol{u}^{+} - \nabla p^{+}\right\}\cdot\boldsymbol{u}'dVdt \\
=& -\int_t\int_V \frac{\partial}{\partial t}\left(\boldsymbol{u}'\cdot\boldsymbol{u}^{+}\right)dVdt \\
&+\int_t\int_V \nabla\cdot\left[-\boldsymbol{U}\left(\boldsymbol{u}'\cdot\boldsymbol{u}^{+}\right) + \boldsymbol{u}'p^{+} - \boldsymbol{u}^{+}p' + \frac{1}{Re}\left\{\left(\nabla\boldsymbol{u}'\right)^{T}\cdot\boldsymbol{u}^{+} - \left(\nabla\boldsymbol{u}^{+}\right)^{T}\cdot\boldsymbol{u}'\right\}\right]dVdt.
\end{aligned} \tag{A-11}$$

The second term on the right side is eliminated by boundary conditions. The first term is expressed as

$$\int_t\int_V \frac{\partial}{\partial t}\left(\boldsymbol{u}'\cdot\boldsymbol{u}^{+}\right)dVdt = \int_V \left[\boldsymbol{u}'\cdot\boldsymbol{u}^{+}\right]_0^T dV = \int_V \boldsymbol{u}'(T)\cdot\boldsymbol{u}^{+}(T)dV - \int_V \boldsymbol{u}'(0)\cdot\boldsymbol{u}^{+}(0)dV \tag{A-12}$$

Therefore, satisfying $(A-8)$ can be replaced by satisfying the following expression.

$$\int_V \boldsymbol{u}'(T)\cdot\boldsymbol{u}^{+}(T)dV = \int_V \boldsymbol{u}'(0)\cdot\boldsymbol{u}^{+}(0)dV \tag{A-13}$$

Here we introduce a new operator. The time evolution operator of direct and adjoint systems is defined as B, B^{+} and then, $B\left(s\right)\boldsymbol{u}'\left(t\right) = \boldsymbol{u}'\left(t+s\right)$. The following relationship is satisfied as

$$\int_V B\boldsymbol{u}'\cdot\boldsymbol{u}^{+}dV = \int_V \boldsymbol{u}'\cdot B^{+}\boldsymbol{u}^{+}dV. \tag{A-14}$$

By using above, the left side of $(A-13)$ can be written as

$$\int_V \boldsymbol{u}'(T)\cdot\boldsymbol{u}^{+}(T)dV = \int_V B(T)\boldsymbol{u}'(0)\cdot\boldsymbol{u}^{+}(T)dV = \int_V \boldsymbol{u}'(0)\cdot B^{+}(T)\boldsymbol{u}^{+}(T)dV \tag{A-15}$$

and the following expression is satisfied in terms of the adjoint time evolution operator B^+,

$$B^+(T)\,\boldsymbol{u}^+(T) = \boldsymbol{u}^+(0)\,. \tag{A-16}$$

This means that the adjoint system represents the inverse time evolution. Summarizing the above, the adjoint LNSE is written as

$$A^+\boldsymbol{q}^+ = 0 \tag{A-17}$$

and following equations

$$\begin{aligned} -\frac{\partial \boldsymbol{u}^+}{\partial t} - \boldsymbol{U}\cdot\nabla\boldsymbol{u}^+ + (\nabla\boldsymbol{U})^T\cdot\boldsymbol{u}^+ &= -\nabla p^+ + \frac{1}{Re}\Delta\boldsymbol{u}^+ && \text{(A-18)}\\ \nabla\cdot\boldsymbol{u}^+ &= 0. && \text{(A-19)} \end{aligned}$$

Solving these equations, we consider carrying out the time evolution from $t = T$ to $t = 0$ where T is the period of invariant solution. Then, we define $\bar{t} = T - t$ and solve the equations from $\bar{t} = 0$ to $\bar{t} = T$. Therefore, we rewrite $(A-18)$ and $(A-19)$ to following as

$$\begin{aligned} \frac{\partial \boldsymbol{u}^+}{\partial \bar{t}} - \boldsymbol{U}\cdot\nabla\boldsymbol{u}^+ + (\nabla\boldsymbol{U})^T\cdot\boldsymbol{u}^+ &= -\nabla p^+ + \frac{1}{Re}\Delta\boldsymbol{u}^+ && \text{(A-20)}\\ \nabla\cdot\boldsymbol{u}^+ &= 0. && \text{(A-21)} \end{aligned}$$

Numerical method

As in the substitute of equations (2.6)-(2.8), we solve following equations about the direct LNSE.

$$\begin{aligned} \frac{\partial \Delta u'_y}{\partial t} &= -\left(\nabla\times\left(\nabla\times\left(\boldsymbol{U}\times\boldsymbol{\omega}' + \boldsymbol{u}'\times\boldsymbol{\Omega}\right)\right)\right)_y + \frac{1}{Re}\left(\Delta^2 u'_y\right) && \text{(A-22)}\\ \frac{\partial \omega'_y}{\partial t} &= \left(\nabla\times\left(\boldsymbol{U}\times\boldsymbol{\omega}' + \boldsymbol{u}'\times\boldsymbol{\Omega}\right)\right)_y + \frac{1}{Re}\Delta\omega'_y && \text{(A-23)}\\ \frac{\partial}{\partial t}\frac{\partial^2\phi'_x}{\partial y^2} &= \frac{\partial}{\partial y}\left\langle\left(\boldsymbol{U}\times\boldsymbol{\omega}' + \boldsymbol{u}'\times\boldsymbol{\Omega}\right)_x\right\rangle_{xz} + \frac{1}{Re}\frac{\partial^4\phi'_x}{\partial y^4} && \text{(A-24)}\\ \frac{\partial}{\partial t}\frac{\partial^2\phi'_z}{\partial y^2} &= \frac{\partial}{\partial y}\left\langle\left(\boldsymbol{U}\times\boldsymbol{\omega}' + \boldsymbol{u}'\times\boldsymbol{\Omega}\right)_z\right\rangle_{xz} + \frac{1}{Re}\frac{\partial^4\phi'_z}{\partial y^4} && \text{(A-25)} \end{aligned}$$

Boundary conditions are given as

$$u'_y = \omega'_y = \frac{\partial u'_y}{\partial y} = \frac{\partial \phi'_x}{\partial y} = \frac{\partial \phi'_z}{\partial y} = 0. \tag{A-26}$$

Considering about the adjoint LNSE, here the nonlinear terms of $(A-20)$ is rewritten as

$$-\left(\boldsymbol{U}\cdot\nabla\right)\boldsymbol{u}^+ + (\nabla\boldsymbol{U})^T\cdot\boldsymbol{u}^+ = \boldsymbol{U}\times\boldsymbol{\omega}^+ + \nabla\left(\boldsymbol{U}\cdot\boldsymbol{u}^+\right) - 2\left(\nabla\boldsymbol{u}^+\right)^T\cdot\boldsymbol{U} \tag{A-27}$$

and following equations are given as

$$\frac{\partial \Delta u_y^+}{\partial \bar{t}} = -\left(\nabla \times \left(\nabla \times \left(-\left(\boldsymbol{U} \times \boldsymbol{\omega}^+\right) + 2\left(\nabla \boldsymbol{u}^+\right)^T \cdot \boldsymbol{U}\right)\right)\right)_y + \frac{1}{Re}\left(\Delta^2 u_y^+\right) \tag{A-28}$$

$$\frac{\partial \omega_y^+}{\partial \bar{t}} = \left(\nabla \times \left(-\left(\boldsymbol{U} \times \boldsymbol{\omega}^+\right) + 2\left(\nabla \boldsymbol{u}^+\right)^T \cdot \boldsymbol{U}\right)\right)_y + \frac{1}{Re}\Delta \omega_y^+ \tag{A-29}$$

$$\frac{\partial}{\partial \bar{t}}\frac{\partial^2 \phi_x^+}{\partial y^2} = \frac{\partial}{\partial y}\left\langle \left(-\left(\boldsymbol{U} \times \boldsymbol{\omega}^+\right) + 2\left(\nabla \boldsymbol{u}^+\right)^T \cdot \boldsymbol{U}\right)_x \right\rangle_{xz} + \frac{1}{Re}\frac{\partial^4 \phi_x^+}{\partial y^4} \tag{A-30}$$

$$\frac{\partial}{\partial \bar{t}}\frac{\partial^2 \phi_z^+}{\partial y^2} = \frac{\partial}{\partial y}\left\langle \left(-\left(\boldsymbol{U} \times \boldsymbol{\omega}^+\right) + 2\left(\nabla \boldsymbol{u}^+\right)^T \cdot \boldsymbol{U}\right)_z \right\rangle_{xz} + \frac{1}{Re}\frac{\partial^4 \phi_z^+}{\partial y^4}. \tag{A-31}$$

Boundary conditions are given as

$$u_y^+ = \omega_y^+ = \frac{\partial u_y^+}{\partial y} = \frac{\partial \phi_x^+}{\partial y} = \frac{\partial \phi_z^+}{\partial y} = 0. \tag{A-32}$$

Acknowledgments

First of all, I would like to express the greatest appreciation to my supervisor Professor Genta Kawahara for his continuous support and guidance. I would also like to thank my sub-chief examiner of this thesis: Professor Susumu Goto and Professor Kazuyasu Sugiyama for their support, valuable feedback and comments. I would like to express my great gratitude to Assistant Professor Masaki Shimizu for shearing with me his vast knowledge of dynamical systems and his sophisticated program code for the DNS of plane channel flow and Assistant Professor Hideshi Ishida for motivating me by his meaningful comments. My appreciation also goes to Professor Luca Brandt. He welcomed me to his laboratory at Royal Institute of Technology (KTH) and shear with me his knowledge to pursue my work.

I want to thank Dr. Tatsuya Yasuda and Dr. Eiichi Sasaki for their comments and Mr. Shingo Motoki and Mr. Yasufumi Horimoto for their discussion and our encouragement. I would like to thank my colleagues and friends for spending with me precious time and supporting me. Finally, I would like to express my appreciation to my family for their continuous support.

List of publications

Publication

1. T. Kanazawa, M. Shimizu and G. Kawahara, "Sustaining and growing mechanism of localized turbulent band in plane channel flow," to be submitted.

2. T. Kanazawa, M. Shimizu and G. Kawahara, "Growing process of localized turbulence in plane channel flow," to be submitted.

3. M. Shimizu, T. Kanazawa and G. Kawahara, "Exponential growth of lifetime of localized turbulence with its extent in channel flow, " Fluid Dynamics Research, 100598, 2018.

International conferences

1. T. Kanazawa, M. Shimizu and G. Kawahara, "Two-dimensionally localized turbulence in plane channel flow," The Ninth JSME-KSME Thermal and Fluids Engineering Conference, Okinawa, Japan, October 28–30, 2017(oral presentation).

2. T. Kanazawa, M. Shimizu and G. Kawahara, "Exponential increase of the lifetime with the number of coherent structure," 24th International Congress of Theoretical and Applied Mechanics, Palais des congress, Montreal, Canada, August 21–26, 2016(oral presentation).

3. T. Kanazawa, M. Shimizu and G. Kawahara, "Strong dependence of the lifetime on the domain size in plane channel flow," International Symposium on Near-Wall Flows: Transition and Turbulence, Maskawa Building for Education and Research, Kyoto University, Japan, June 20–22, 2016(poster presentation).

4. T. Kanazawa, M. Shimizu and G. Kawahara, "Subcritical transition to turbulence in plane channel flow," ASME-JSME-KSME Joint Fluid Engineering Conference 2015, COEX, Seoul, Korea, July 26–31, 2015(oral presentation).

Domestic conferences

1. T. Kanazawa, M. Shimizu and G. Kawahara, "A sustaining mechanism of an isolated turbulent band in plane channel flow," JSME Fluids Engineering Division, Yamaguchi University, November 12–13, 2016.

2. T. Kanazawa, M. Shimizu and G. Kawahara, "An equilibrium state of an isolated turbulent band in plane channel flow," Annual Meeting, The Japan Society of Fluid Mechanics, Nagoya Institute of Technology, September 23–26, 2016.

3. T. Kanazawa, M. Shimizu and G. Kawahara, "An isolated turbulent band in plane channel flow," Annual Meeting, The Physical Society of Japan, Kanazawa University, September 13–16, 2016.

4. T. Kanazawa, M. Shimizu and G. Kawahara, "Structural dependence of lifetime of localized turbulence in plane channel flow," JSME Fluids Engineering Division, Tokyo University of Science, November 7–8, 2015.

5. T. Kanazawa, M. Shimizu and G. Kawahara, "Transition to turbulence in plane channel flow," JSME Fluids Engineering Division, University of Toyama, October 25–16, 2014.

Workshop

1. T. Kanazawa, M. Shimizu and G. Kawahara, "Domain size dependence of the lifetime and the transition in plane channel flow," RIMS Camp-Style Seminar: Dynamics of wall-bounded shear flows, Kansai Seminar House, Kyoto, August 31-September 2, 2016.

2. T. Kanazawa, M. Shimizu and G. Kawahara, "Strong dependence of the lifetime and the transition with the domain size in plane channel flow," France-Japan Workshop, ESPCI, Paris, France, March 1-3 2016.

3. T. Kanazawa, M. Shimizu and G. Kawahara, "Subcritical Transition to Turbulence in Plane Channel Flow," France-Japan Workshop, Osaka University, Japan, November 11, 2014.